

Synthesis and Characterization of Enantiomeric *anti*-2-Fluorobenzo[*a*]pyrene-7,8-dihydrodiol-9,10-epoxides and Their 2'-Deoxyguanosine and Oligodeoxynucleotide Adducts

Tianle Yang, Yanhe Huang, and Bongsup P. Cho*

Department of Biomedical and Pharmaceutical Sciences, College of Pharmacy, University of Rhode Island,
41 Lower College Road, Kingston, Rhode Island 02881

Received November 7, 2005

Benzo[*a*]pyrene diol epoxides (BPDEs) are the ultimate carcinogenic species of benzo[*a*]pyrene, a prototype polycyclic aromatic hydrocarbon (PAH). BPDE-modified DNA duplexes can adopt multiple conformations depending on the nature of the modified bases, the stereochemistry at the location of the covalent linkage, and the sequence context surrounding the lesion site. In this paper, we describe the preparation of enantiomeric 2-fluoro-BPDEs, *trans*-(7*R*,8*S*)-dihydroxy-(9*S*,10*R*)- and *trans*-(7*S*,8*R*)-(9*R*,10*S*)-epoxy-7,8,9,10-tetrahydro-2-fluorobenzo[*a*]pyrene (**22** and **23**, respectively), as models for probing the BPDE-induced conformational heterogeneity. The multistep synthesis of the target diol epoxides described herein entails regioselective succinylation of 2-fluoropyrene, followed by a ring closure, regio- and stereospecific construction of the 7,8-dihydrodiol functionality, and a subsequent *meta*-chloroperbenzoic acid-mediated epoxidation. Stereoselectivity was achieved by using Jacobsen chiral catalysts, which produced greater than ~90% enantiomeric excess. Absolute configurations at the C_{7,8} carbons of the FBP derivatives were determined by comparison of the circular dichroism (CD) spectra with those reported for the BP analogues. Analysis of the ³J_{7,8} vicinal coupling constants, CD shape, and charge density calculations all indicated that the prepared *anti*-FBPDEs preferentially adopt the pseudo-diequatorial C_{7,8} diol conformation. Hydrolysis of *anti*-FBPDEs produced a 9:1 ratio of *trans*- to *cis*-opened tetraols. Reactions of each of the *anti*-FBPDEs with deoxyguanosine 5'-monophosphate produced predominantly *trans-anti-N*²-dG as the major adducts. Analogous reactions with two 11-mer oligodeoxynucleotides (5'-CCATXGCTACC-3' where X = dT, dC) gave FBP-modified oligodeoxynucleotides with structures that were characterized by enzyme digest/HPLC and electrospray ionization time-of-flight mass spectrometry data. The oligonucleotide adducts were annealed with the appropriate sequences to form fully complementary duplexes [(5'-CCATXG*CTACC-3')(5'-GGTAGCYATGG-3'), G* = FBP-*N*²-dG adduct, X = dT, Y = dA in duplex I; X = dC, Y = dG in duplex II] for CD and UV melting studies. The results of the present study were consistent with those reported previously for BPDE-modified duplexes in the same sequence contexts and support the utility of FBPDEs as useful structural probes.

Introduction

Most chemical carcinogens require metabolic activation *in vivo* to form DNA adducts (*I*). A large number of carcinogen-DNA adducts have been isolated from target tissues and used as biomarkers for cancer diagnosis and chemoprevention research (2–4). Arylamines and polycyclic aromatic hydrocarbons (PAH)¹ are the major groups of bulky carcinogens that produce DNA adducts (*I*, 5–7). The great complexity of DNA adduct structures, however, has impeded the elucidation of an unambiguous structure–mutation relationship at the molecular–genetic level (6–8). This is due, in part, to the fact that bulky adducts in DNA exist frequently as conformeric mixtures (9, 10). Moreover, the dynamics of multiple conformations are modulated by the adduct structures and the base sequences

surrounding the lesion, termed adduct- and sequence-induced conformational heterogeneities, respectively (*II*). The relatively small energy differences among the conformers enable conformation switches to occur readily in the active sites of repair or with replication enzymes, which makes it difficult to identify which conformation is responsible for which mutation.

Benzo[*a*]pyrene (BP), an extensively studied PAH, undergoes metabolic activation *in vivo* that transforms it into highly tumorigenic diol epoxides {benzo[*a*]pyrene-7,8-dihydrodiol-9,10-epoxide (BPDE)}, which bind covalently with purine bases to form stable DNA adducts (*I*). Extensive structural studies have shown that BPDE-modified DNAs adopt three major types of conformations: base displacement, minor groove, and classical intercalation (9, 11). The relative prevalence of these conformations varies depending on the nature of the modified base, the location of the covalent linkage, and the base sequence context surrounding the lesion site. For example, all PAH-dA adducts that have been studied thus far universally adopt a classical intercalation conformation. Meanwhile, PAH-dG adducts usually adopt either a minor groove or base displacement conformation or possibly a combination of the two, depending on the nature of the epoxide opening and the base sequence context. The size, the topology, and the stereochemistry of the

* To whom correspondence should be addressed. Tel: 401-874-5024. Fax: 401-874-5766. E-mail: bcho@uri.edu.

¹ Abbreviations: BP, benzo[*a*]pyrene; BPDE, benzo[*a*]pyrene-7,8-dihydrodiol-9,10-epoxide; CD, circular dichroism; DDQ, 2,3-dichloro-5,6-dicyano-1,4-benzoquinone; ESI-TOF-MS, electrospray ionization time-of-flight mass spectrometry; FBPDE, 2-fluorobenzo[*a*]pyrene-7,8-dihydrodiol-9,10-epoxide; FBPT, 2-fluorobenzo[*a*]pyrene-7,8,9,10-tetraol; ICD, induced circular dichroism; mCPBA, *meta*-chloroperbenzoic acid; PAH, polycyclic aromatic hydrocarbon.

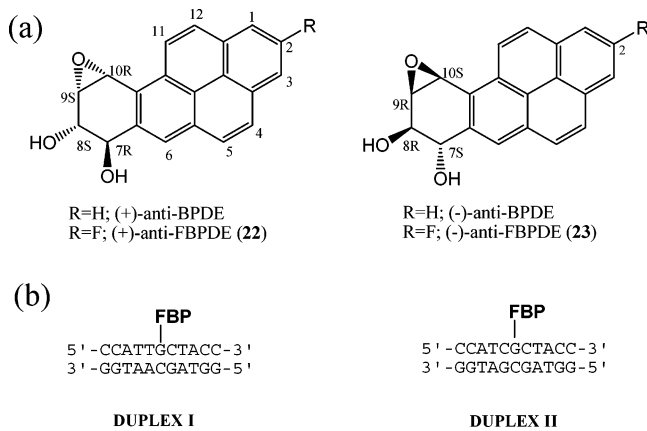


Figure 1. Structures of (a) (+)- and (-)-anti-BPDE and the corresponding anti-FBPDE derivatives: *trans*-7*R*,8*S*-dihydroxy-9*S*,10*R*-epoxy-7,8,9,10-tetrahydro-2-fluorobenzo[*a*]pyrene (**22**) and *trans*-7*S*,8*R*-dihydroxy-9*R*,10*S*-epoxy-7,8,9,10-tetrahydro-2-fluorobenzo[*a*]pyrene (**23**). (b) Base sequence contexts of FBP-modified 11-mer duplexes I and II.

carcinogens are all important factors that further diversify adduct conformation (12).

We have been exploring ^{19}F NMR spectroscopy as an alternative to ^1H NMR spectroscopy for probing the conformational heterogeneities induced by arylamine carcinogens, such as 4-aminobiphenyl, 2-aminofluorene, and *N*-acetyl-2-aminofluorene (13, 14). Although the levels of structural detail that can be observed with ^1H NMR cannot be matched with ^{19}F NMR, the sensitivity of the ^{19}F nucleus to the macromolecular environment and the lack of background noise associated with ^{19}F NMR present unique advantages for the investigation of the complex conformational dynamics of adduct- and sequence-induced heterogeneity (11). We therefore initiated a program to investigate the sequence-dependent conformational heterogeneity in BPDE mutagenesis, which is an endeavor that requires preparation of fluorine-containing BPDEs as model probes. In this paper, we first describe a multistep stereospecific synthesis and characterization of enantiomeric anti-2-fluorobenzo[*a*]pyrene-7,8-dihydrodiol-9,10-epoxides (anti-FBPDE, **22** and **23**, respectively) (Figure 1a). Hydrolysis of each of the anti-FBPDEs to its respective fluorobenzo[*a*]pyrene tetraols (FBPTs) was also studied. Second, we describe the reactions of the FBPDEs with deoxyguanosine 5'-monophosphate (dGMP) and 11-mer oligodeoxynucleotides (5'-CCATXGCTACC-3' where X = dC, dT), as well as their characterization by electrospray ionization time-of-flight mass spectrometry (ESI-TOF-MS), enzyme digestion/HPLC, and circular dichroism (CD). The modified oligodeoxynucleotides were annealed with complementary sequences to form duplexes (duplexes I and II, Figure 1b) and their thermodynamic (UV melting) and conformational (CD) properties were investigated.

Experimental Procedures

Materials. All organic solvents and reagents were purchased from Aldrich (Milwaukee, WI) and Fisher Scientific (Pittsburgh, PA) and used without further purification unless noted otherwise. Anhydrous tetrahydrofuran (THF) was prepared from a fresh distillation from sodium and benzophenone. Anhydrous benzene was freshly distilled from CaH_2 . Column chromatography was performed on silica gel 60 (0.063–0.200 μm) (Scientific Adsorbents Inc., Atlanta, GA). Oligonucleotides were purchased in desalted forms from Sigma-Genosys (The Woodlands, TX). Enzymes used in digestion experiments (DNase I, phosphodiesterase I, and alkaline phosphatase) were all obtained from Sigma Chemical (Milwaukee,

WI). 4,5,9,10-Tetrahydropyrene (**1**), 2-nitropyrene (**3**), 2-aminopyrene (**4**), and 6-fluoropyrene were prepared according to the modified literature procedures (Supporting Information).

Instrumentation. The HPLC system consists of a Hitachi EZChrom Elite HPLC system with a L2450 diode array as a detector. The purification system employed a mobile phase system involving acetonitrile in pH 7.0 ammonium acetate buffer (0.10 M) with a flow rate of 2.0 mL/min. Specific column and gradient conditions are described in the appropriate experimental sections. Uncorrected melting points were determined on a Buchi 535 melting point apparatus. Elemental analyses were performed by M-H-W Laboratories (Phoenix, AZ). High (HRMS) and low (LRMS) resolution electron impact mass spectra were obtained at the University of Illinois Mass Spectrometry Laboratory (Urbana-Champaign, IL). A Mariner Biospectrometry Workstation (Foster City, CA) was used to obtain electrospray mass spectra. ^1H , ^{13}C , and ^{19}F NMR spectra were recorded on a Bruker NMR spectrometer operating at 400 MHz (DPX Avance). ^1H and ^{13}C chemical shifts are expressed in ppm with respect to the internal standard tetramethylsilane. ^{19}F NMR spectra were referenced to CFCl_3 by assigning external hexafluorobenzene in C_6D_6 at -164.90 ppm. Hydrogenation was performed on a Parr hydrogenation apparatus at room temperature.

CD. CD measurements were conducted on a Jasco J-810 spectropolarimeter equipped with a variable Peltier temperature controller. Data were analyzed by the programs (Spectral and Interval Analyses) provided by the manufacturer. All CD experiments were conducted at 15 $^\circ\text{C}$. Typically, ~ 2 ods of a duplex sample were dissolved in 0.2 M NaCl, 10 mM sodium phosphate, and 0.2 mM EDTA, pH 7.0, and placed in a 1 mm path length cell and heated at 85 $^\circ\text{C}$ for 5 min and then cooled to 15 $^\circ\text{C}$ over a 10 min period. The spectropolarimeter was scanned from 200 to 500 nm at a rate of 50 nm/min. Data points were acquired every 0.2 nm with a 2 s response time and sensitivity in the range of 4–10 mdeg. Spectra were the averages of 10 accumulations and smoothed using 17 point adoptive smoothing algorithms provided by Jasco.

UV Melting Experiments. Melting curves were measured by using a Beckman DU 800 UV/VIS spectrophotometer equipped with a six chamber, 1 cm path length T_m cells. Sample cell temperatures were controlled by a built-in Peltier temperature controller. Duplexes with a total concentration in the range of 0.2–14 μM were prepared in 0.2 M NaCl, 10 mM sodium phosphate, and 0.2 mM EDTA, at pH 7.0. Samples were initially degassed by heating at 85 $^\circ\text{C}$ for 5 min, and subsequent annealing was achieved by slow cooling over a 30 min period to 15 $^\circ\text{C}$. Melting curves were constructed by varying the temperature of the sample cell (1 $^\circ\text{C}/\text{min}$) and monitoring the absorbance of the sample at 260 nm. A typical melting experiment consisted of two forward and two reverse scans and was repeated three times. Thermodynamic parameters for bimolecular melting reactions for the duplex were obtained from melting curve data using the program MELTWIN version 3.5. Two different methods were used to calculate the enthalpy (ΔH°) and entropy (ΔS°) of the coil-helix equilibrium: (a) fits of individual curves and (b) plots of T_m^{-1} vs $\ln C_t$ to fit to $T_m^{-1} = R/\Delta H^\circ \ln C_t/4 + \Delta S^\circ/\Delta H^\circ$, in which T_m is a melting transition point in K and R is the gas constant (1.987 cal/kmol). The margin of agreement between the parameters derived from curve fit and $T_m^{-1} - \ln C_t$ plots are within the 15% range; thus, their average values are listed in Table 2.

Synthesis. 2-Fluoropyrene (5). To a THF solution of 2-aminopyrene (236 mg, 1.1 mmol) and $(\text{Et}_2\text{O})\text{BF}_3$ (278 μL) was added 220 μL of *t*-BuONO at -8 $^\circ\text{C}$. After the mixture was stirred for 1 h, 50 mL of pentane was added and the solid material was precipitated. The mixture was filtered and washed with ether to obtain a crude tetrafluoroboron-diazonium salt, which was then dried by vacuum. The dried diazonium salt was heated in xylenes at reflux for 1 h. Evaporation of the solvent gave a solid residue, which was purified by column on silica (hexanes) to give 2-fluoropyrene as a pure white solid (97 mg, 44%); mp 148–149 $^\circ\text{C}$ (ethanol). ^1H NMR (CDCl_3): δ 7.85 (d, $J_{1,F}$, $J_{3,F} \sim 9.5$ Hz, $\text{H}_{1,3}$,

2H), 7.99 (t, $J_{6,7} = 7.6$ Hz, H₇, 1H), 8.01 (d, $J = 9.0$ Hz, 2H), 8.10 (d, $J = 9.0$ Hz, 2H), 8.20 (d, $J = 7.6$ Hz, H_{6,8}, 2H). ¹⁹F NMR (CDCl₃): δ -114.99 (apparent t, $^3J_{H-F} = 11.3$, 7.5 Hz). 1-Fluoropyrene was prepared similarly by Schiemann reaction of 1-aminopyrene, which in turn was obtained from reduction (NH₂NH₂/Pd/C) of commercially available 1-nitropyrene (60% yield). ¹H NMR (acetone-*d*₆): δ 8.29 (m, $J = 7.7$ Hz, 4H), 8.18 (s, 3H), 8.07 (d, $J = 14.7$ Hz, H₂, 1H), 8.02 (d, $J = 7.0$ Hz, H₃, 1H).

4-[1-(7-Fluoropyrenyl)-1-oxo-butanoic Acid (6). 2-Fluoropyrene (**5**, 1.5 g, 6.7 mmol) was treated with anhydrous AlCl₃ (3.3 g, 23 mmol) and succinic anhydride (0.80 g, 8.0 mmol) in nitrobenzene (12 mL). The mixture was stirred overnight under N₂. Concentrated HCl (3 mL) was added to the dark brown solution, and the mixture was distilled to remove nitrobenzene. The remaining mixture was filtered and washed with dilute HCl and water. The crude solid obtained after the usual workup was purified by column chromatography using chloroform as a solvent to give **6** as an off-white solid (2.0 g, 94%); mp 199–200 °C. ¹H NMR (DMSO-*d*₆): δ 2.75 (t, $J_{12,13} = 6.2$ Hz, H₁₃, 2H), 3.57 (t, $J_{12,13} = 6.2$ Hz, H₁₂, 2H), 8.13 (d, $J_{1,F}$, $J_{3,F} \sim 9.6$ Hz, H_{1,3}, 2H), 8.28 (d, $J_{7,8} = 9.5$ Hz, H₈, 1H), 8.29 (s, 2H), 8.42 (d, $J = 8.1$ Hz, 1H), 8.59 (d, $J = 8.1$ Hz, 1H), 8.89 (d, $J_{7,8} = 9.5$ Hz, H₇, 1H), 12.22 (s, COOH, 1H). ¹³C NMR (DMSO-*d*₆): δ 203.29 (C₁₁), 173.88 (COOH), 160.27 (d, $J_{2,F} = 242.0$ Hz, C₂), 133.38, 132.80 (d, $J_{10a,F}$ or $3a,F = 10.0$ Hz), 132.27, 131.99 (d, $J_{10a,F}$ or $3a,F = 10.0$ Hz), 128.56, 128.51, 128.39 (d, $J = 3.8$ Hz), 127.33, 126.12, 125.78, 125.30, 123.63, 120.60, 112.31 (d, $J_{1,F}$ or $3,F = 23.1$ Hz), 111.73 (d, $J = 9.2$, 9.2 Hz). ¹⁹F NMR (acetone-*d*₆): δ -114.99 (apparent t, $^3J_{H-F} = 9.2$, 9.2 Hz). LRMS (70 eV): m/z (%) 320.1 (17, M⁺), 302.0 (33), 274.1 (22), 247.0 (100), 219.0 (75), 109.2 (25). HRMS calcd for C₂₀H₁₃O₃F, 320.0849; found, 320.0856.

4-[1-(7-Hydroxypyrenyl)]butanoic Acid (7). A solution of the keto-acid **6** (320 mg, 1 mmol), KOH (930 mg), and 1.5 mL of hydrazine in 7 mL of diethylene glycol was mixed and heated at reflux under N₂ for 4 h. The solution was then adjusted to pH 1.0 with 6 N HCl and extracted with ethyl acetate. The combined organic extracts were washed with water and dried over anhydrous MgSO₄. The residue after solvent evaporation was purified by silica column chromatography to furnish the phenolic product **7** as a pale yellow solid (252 mg, 83%); mp 225–226 °C. ¹H NMR (DMSO-*d*₆): δ 1.96–2.00 (m, H₁₂, 2H), 2.36 (t, $J_{12,13} = 7.2$ Hz, H₁₃, 2H), 3.29 (t, $J_{11,12} = 8$ Hz, H₁₁, 2H), 8.29 (d, $J = 9.3$ Hz, 1H), 8.12 (d, $J = 7.7$ Hz, H₈, 1H), 8.01–8.05 (m, 2H), 7.94 (d, $J = 9.0$ Hz, 1H), 7.79 (d, $J = 7.8$ Hz, H₇, 1H), 7.64 (d, $J_{1,3} = 2.0$ Hz, H₁ or 3 , 1H), 7.63 (d, $J_{1,3} = 2.0$ Hz, H₁ or 3 , 1H). ¹³C NMR (DMSO-*d*₆): δ 175.33, 156.77, 112.43, 112.77, 137.29, 133.50, 132.99, 129.09, 128.65, 127.86, 127.47, 126.97, 126.76, 125.89, 125.35, 124.62, 119.63, 34.30, 32.92, 27.77. LRMS (70 eV): m/z (%) 304.1 (65, M⁺), 244.1 (10), 231.1 (100), 215.1 (5), 202.1 (17), 115.6 (3). Elemental analysis calcd for C₂₀H₁₆O₃: C, 78.93; H, 5.30. Found: C, 78.83; H, 5.54.

4-[1-(7-Fluoropyrenyl)]butanoic Acid (8). A mixture of **6** (1.6 g, 5 mmol), red phosphorus (0.77 g), and hydriodic acid (HI, 55%, 9.2 mL) in acetic acid (30 mL) was heated to reflux under N₂ for 72 h. The mixture was quenched with water, and the solid was filtered. The crude product was purified by silica column chromatography (hexane and ethyl acetate) to give the acid product **8** as a pale yellow solid (1.63 g, 76%); mp 190–191 °C (ethanol). ¹H NMR (DMSO-*d*₆): δ 2.19–2.25 (m, H₁₂, 2H), 2.53 (t, $J_{12,13} = 7.2$ Hz, H₁₃, 2H), 3.43 (t, $J_{11,12} = 6.4$ Hz, H₁₁, 2H), 7.84 (d, $J_{1,F}$, $J_{3,F} \sim 9.6$ Hz, H_{1,3}, 2H), 7.87 (d, $J = 7.8$ Hz, H₇, 1H), 7.97 (d, $J = 8.9$ Hz, 1H), 8.06 (d, $J = 9.3$ Hz, 1H), 8.08 (d, $J = 8.9$ Hz, 1H), 8.15 (d, $J = 7.8$ Hz, H₈, 1H), 8.35 (d, $J = 9.4$ Hz, 1H), 12.2 (s, 1H). ¹³C NMR (DMSO-*d*₆): δ 174.46 (COOH), 160.71 (d, $J = 241.9$ Hz, C₂), 137.41, 132.97 (d, $J = 10.1$ Hz, C_{10a} or $3a$), 132.44 (d, $J = 9.9$ Hz, C_{10a} or $3a$), 128.88, 128.67, 127.53, 127.40, 126.57 (d, $J = 3.7$ Hz), 125.87, 125.81, 124.88, 123.88, 121.22, 110.82 (d, $J = 23.4$ Hz), 110.59 (d, $J = 23.3$ Hz), 33.37 (C₁₁), 32.04 (C₁₃), 26.96 (C₁₂). ¹⁹F NMR (acetone-*d*₆): δ -116.45 (apparent t, $^3J_{H-F} = 9.8$, 9.8 Hz). LRMS (70 eV): m/z (%) 306.1 (42, M⁺), 233.0 (100). HRMS calcd for C₂₀H₁₅O₂F, 306.1060; found, 306.1056.

9,10-Dihydro-2-fluorobenzo[a]pyren-7(8H)-one (9). Compound **8** (612 mg, 2 mmol) was placed in a gastight Daiflon (polytrifluoromonochloroethylene) HF delivery system in a well-ventilated hood. Approximately 10 mL of pure HF was added to the reaction vessel, and the reaction mixture was stirred under N₂ overnight in a closed system at room temperature. The excess HF was removed by flushing with dry N₂. The remaining dark black residue was treated with aqueous KOH solution overnight. The aqueous suspension was extracted with methylene chloride, and the combined extracts were washed successively with dilute KOH and water and finally dried over anhydrous MgSO₄. The organic residue after solvent evaporation was subjected to silica column chromatography (hexanes and ethyl acetate) followed by recrystallization from benzene and ethanol to furnish the cyclized product **9** as an off-white solid (550 mg, 96%); mp 169–170 °C (ethanol). ¹H NMR (CDCl₃): δ 2.18 (m, H₉, 2H), 2.71 (t, $J_{8,9} = 5.8$ Hz, H₈, 2H), 3.51 (t, $J_{9,10} = 6.3$ Hz, H₁₀, 2H), 7.78 (d, H_{1,3}, $J_{1,F}$, $J_{3,F} \sim 10$ Hz, 2H), 7.88 (d, $J = 9.0$ Hz, 1H), 8.00 (d, $J = 9.3$ Hz, 1H), 8.04 (d, $J = 9.0$ Hz, 1H), 8.26 (d, $J = 9.3$ Hz, 1H), 8.83 (s, H₆, 1H). ¹³C NMR (CDCl₃): δ 198.96 (C₇), 161.32 (d, $J = 246.1$ Hz, C₂), 138.50, 134.06 (d, $J = 9.7$ Hz), 133.36 (d, $J = 9.8$ Hz), 129.59, 128.67, 127.81, 127.13 (d, $J = 3.7$ Hz), 126.76, 126.59 (d, $J = 3.7$ Hz), 124.40, 124.02, 121.31, 111.71 (d, $J = 12.9$ Hz), 111.04 (d, $J = 12.7$ Hz), 92.21, 38.79, 26.14, 23.00. ¹⁹F NMR (CDCl₃): δ -112.99 (apparent t, $^3J_{H-F} = 11.3$, 7.5 Hz). LRMS (70 eV): m/z (%) 288.1 (100, M⁺), 232.1 (65), 168.1 (11), 115.3 (21), 77 (20). HRMS calcd for C₂₀H₁₃O₂F, 288.0950; found, 288.0951.

9,10-Dihydro-2-fluorobenzo[a]pyrene (10). To a solution of **9** (864 mg, 3 mmol) in THF (15 mL) and EtOH (30 mL) was added NaBH₄ (800 mg, 21 mmol) slowly over a period of 20 min. After it was stirred at room temperature for 2 h, the reaction was quenched by the addition of water and the organic solvents were removed under reduced pressure. The resulting organic residue was dissolved in ether, and the combined ether extracts were washed with water and dried over anhydrous MgSO₄. The crude alcohol was refluxed for 3 h in dry benzene (70 mL) containing a catalytic amount of *p*-toluenesulfonic acid. The solution was cooled and washed successively with saturated sodium carbonate and water and saturated NaCl and dried over anhydrous MgSO₄. Evaporation of the solvent furnished **10** as a yellow solid, which was purified by silica column chromatography (hexanes and ethyl acetate) (694 mg, 85%); mp 145–147 °C. ¹H NMR (CDCl₃): δ 2.61 (m, H₉, 2H), 3.47 (t, $J_{9,10} = 8.3$ Hz, H₁₀, 2H), 6.27 (dt, $J_{8,9} = 4.4$ Hz, $J_{7,8} = 9.6$ Hz, H₈, 1H), 6.84 (dt, $J_{7,9} = 1.8$ Hz, $J_{7,8} = 9.5$ Hz, H₇, 1H), 7.77 (dt, $J_{1,3} = 2.7$ Hz, $J_{1,F}$, $J_{3,F} \sim 9.5$ Hz, H_{1,3}, 2H), 7.84–7.99 (m, 4H), 8.35 (d, $J = 9.4$ Hz, H₁₁, 1H). ¹³C NMR (CDCl₃): δ 23.19 (C₉), 23.33 (C₁₀), 110.63 (d, $J_{1,F}$ or $3,F = 22.8$ Hz), 110.88 (d, $J_{1,F}$ or $3,F = 22.8$ Hz), 121.96, 123.82, 124.14, 124.21, 125.84 (d, $J_{12,F}$ or $4,F = 14.4$ Hz), 126.56 (d, $J_{4,F}$ or $12,F = 16.2$ Hz), 127.38, 128.61, 128.70, 128.98, 129.23, 130.46, 131.68, 132.50 (d, $J_{12a,F}$ or $3a,F = 9.8$ Hz), 133.08 (d, $J_{12a,F}$ or $3a,F = 9.8$ Hz), 160.62 (d, $J_{2,F} = 241.6$ Hz, C₂). ¹⁹F NMR (CDCl₃): δ -115.58 (apparent t, $^3J_{H-F} = 11.3$, 7.5 Hz). LRMS (70 eV): m/z (%) 304.1 (16, M⁺), 286.1 (100), 270.1 (73), 257.1 (79), 244.1 (14). HRMS calcd for C₂₀H₁₃O₂F, 304.0900; found, 304.0907. Elemental analysis calcd for C₂₀H₁₃F: C, 83.32; H, 4.83; F, 6.61. Found: C, 83.13; H, 4.84; F, 6.71.

2-Fluorobenzo[a]pyrene (11). A mixture of **10** (27 mg, 0.01 mmol) and DDQ (137 mg, 0.6 mmol) in benzene (4 mL) was heated at reflux overnight. The reaction mixture was poured onto a short column containing neutral (activity I) aluminum oxide. Elution with benzene furnished a yellow residue, which was recrystallized in benzene to give **11** as a bright yellow solid (25 mg, 94%); mp 168–170 °C. ¹H NMR (CDCl₃): δ 7.75–7.88 (m, 5H), 8.03 (d, $J = 9.1$ Hz, H₄ or 5 , 1H), 8.24 (d, $J = 9.1$ Hz, H₄ or 5 , 1H), 8.29 (dd, $J = 3.8$, 7.8 Hz, H₇, 1H), 8.53 (s, H₆, 1H), 9.02 (d, $J = 8.4$ Hz, H₁₀ or 11 , 1H), 9.06 (d, $J = 9.2$ Hz, H₁₀ or 11 , 1H). ¹³C NMR (CDCl₃): δ 160.79 (d, $J = 244.5$ Hz, C₂), 133.67 (d, $J = 10.0$ Hz), 132.82 (d, $J = 9.7$ Hz), 130.99, 129.46, 129.06, 128.99, 128.43, 126.92 (d, $J = 3.5$ Hz), 126.69 (d, $J = 4.2$ Hz), 126.51, 126.32, 126.04, 125.74, 123.42, 123.27, 122.83, 122.27, 111.93 (d, $J =$

23.8 Hz), 110.31 (d, $J = 21.8$ Hz). ^{19}F NMR (CDCl_3): $\delta -114.89$ (apparent t, $^3J_{\text{H-F}} = 11.3, 7.5$ Hz).

trans-(7S,8S)-Dihydroxy-7,8,9,10-tetrahydro-2-fluorobenzo[a]pyrene (12). (*R,R*)-*N,N'*-bis(3,5-di-*tert*-butylsalicylidene)-1,2-cyclohexanediaminomanganese(III) chloride (*R,R*-Jacobsen catalyst) was added to a 10 mL methylene chloride solution containing **10** (136 mg, 0.5 mmol) and 4-phenylpyridine-*N*-oxide (4-PPNO, 22 mg, 0.125 mmol). The mixture was then cooled to -8°C and added slowly to a precooled phosphate-buffered bleach solution (2.7 mL, pH 11.3, 0.6 M). The reaction mixture was stirred for 1 h and then quickly poured into a short silica column and eluted with methylene chloride. The organic solvent was evaporated under reduced pressure to give a crude 7,8-epoxide, which was used directly for the next step without further purification. To a solution of the crude 7*R*,8*S*-epoxide (72 mg, 0.25 mmol) in a 4:1 mixture of acetone and water (6 mL) was added 10-camphorsulfonic acid (4 mg). The mixture was stirred for 3 h at room temperature. The solvent was evaporated, and the residue was partitioned between water and ethyl acetate. The combined organic extracts were washed with water and dried over anhydrous MgSO_4 . Evaporation of the solvent, followed by silica gel purification (methylene chloride and methanol), afforded the tetrahydrodiol **12** as an off-white solid. ^1H NMR (CDCl_3): δ 8.44 (s, H_6 , 1H), 8.25 (d, $J = 9.6$ Hz, 1H), 8.06 (d, $J = 9.6$ Hz, 2H), 7.92 (d, $J = 8.5$ Hz, 1H), 7.81 (d, $J = 10.2$ Hz, $\text{H}_{1,3}$, 2H), 5.01 (m, H_7 , 1H), 4.02 (m, H_8 , 1H), 3.67 (m, H_{10} , 1H), 2.45 (m, H_9 , 1H). LRMS (70 eV): m/z (%) 306.1 (100, M^+), 288.1 (22), 262.1 (54), 233.1 (63), 207.0 (9), 128.4 (7). HRMS calcd for $\text{C}_{20}\text{H}_{15}\text{O}_2\text{F}$, 306.1057; found, 306.1056.

trans-(7R,8R)-Dihydroxy-7,8,9,10-tetrahydro-2-fluorobenzo[a]pyrene (14). LRMS (70 eV): m/z (%) 306.2 (100, M^+), 288.1 (61), 262.1 (42), 246.1 (34), 233.1 (52), 167.1 (25), 149.1 (63), 71.1 (28). HRMS calcd for $\text{C}_{20}\text{H}_{15}\text{O}_2\text{F}$, 306.1057; found, 306.1048.

trans-(7S,8S)-bis(Benzoyloxy)-7,8,9,10-tetrahydro-2-fluorobenzo[a]pyrene (13). A mixture of **12** (73 mg, 0.24 mmol), benzoyl chloride (100 μL), DMAP (3 mg), and pyridine (0.8 mL) in methylene chloride (5 mL) was stirred at room temperature overnight. The mixture was diluted with 100 mL of ether, and the ether layer was washed successively with 10% NaOH and water and dried over anhydrous MgSO_4 . Concentration of the solvent followed by silica column chromatography (hexanes and ethyl acetate) afforded the pure *trans*-dibenzoate **13** as a white solid (113 mg, 91%). ^1H NMR (CDCl_3): δ 2.54 (m, H_9 , 1H), 2.74 (m, H_9 , 1H), 3.71 (m, H_{10} , 2H), 5.79 (m, H_8 , 1H), 6.98 (d, $J_{7,8} = 6.0$ Hz, H_7 , 1H), 7.32–7.63 (m, 8H), 7.78–8.20 (m, 9H). ^{13}C NMR (CDCl_3): δ 166.27 (C=O), 165.98 (C=O), 160.62 (d, $J_{2,\text{F}} = 241.6$ Hz, C_2), 133.74, 133.47, 133.34, 133.27, 133.08, 132.75, 132.63, 131.17, 130.55, 130.22, 129.94, 129.90, 129.70, 129.35, 128.77, 128.47, 128.34, 127.97, 127.17, 127.11, 126.40, 126.33, 124.31, 124.09, 121.47, 111.57 (d, $^3J_{\text{C,F}} = 23.0$ Hz), 110.99 (d, $^3J_{\text{C,F}} = 23.0$ Hz), 72.08, 71.73, 25.02, 23.43.

trans-(7R,8R)-bis(Benzoyloxy)-7,8,9,10-tetrahydro-2-fluorobenzo[a]pyrene (15). LRMS (70 eV): m/z (%) 514.3 (10, M^+), 446.3 (100), 392.3 (13), 270.2 (89), 105.1 (98), 77.1 (43). HRMS calcd for $\text{C}_{34}\text{H}_{23}\text{O}_4\text{F}$, 514.1580; found, 514.1580.

trans-7S,8S-bis(Benzoyloxy)-7,8-dihydro-2-fluorobenzo[a]pyrene (18). Compound **13** (50 mg, 0.1 mmol) was heated at reflux overnight in dry benzene (5 mL) containing DDQ (934 mg, 0.15 mmol). The hot reaction mixture was poured onto a short column containing basic aluminum oxide. Elution with benzene furnished a residue, which was purified additionally by silica column chromatography to give the pure product as a white solid (45 mg, 91%). ^1H NMR (CDCl_3): δ 8.46 (d, $J_{11,12} = 9.4$ Hz, 1H), 8.25 (s, H_6), 7.97–8.14 (m, 5H), 7.86 (d, $J = 9.3$ Hz, 2H), 7.77 (d, $J_{9,10} = 10$ Hz, H_{10} , 1H), 7.34–7.59 (m, 7H), 7.06 (d, $J_{7,8} = 7.5$ Hz, H_7 , 1H), 6.49 (dd, $J_{9,10} = 10$ Hz, $J_{8,9} = 3.6$ Hz, H_9 , 1H), 6.21 (ddd, $J_{8,10} = 1$ Hz, $J_{8,9} = 3.6$ Hz, $J_{7,8} = 7.5$ Hz, H_8 , 1H). ^{13}C NMR (CDCl_3): δ 165.97, 165.94, 159.22 (d, $J = 236.6$ Hz, C_2), 133.63, 133.53, 133.45, 133.14, 132.86, 130.51, 130.45, 130.21, 130.04, 129.93, 129.82, 129.46, 129.04, 128.73, 128.60, 127.92, 127.89, 127.47, 127.43, 126.71, 126.64, 126.59, 126.52, 126.40, 125.06, 123.65, 121.93, 111.99 (d, $J = 23.6$ Hz), 111.76 (d, $J = 23.5$ Hz),

72.78, 71.05. ^{19}F NMR (CDCl_3): $\delta -114.22$ (apparent t, $^3J_{\text{H-F}} = 11.3, 7.5$ Hz). LRMS (70 eV): m/z (%) 512.2 (7, M^+), 446.2 (15), 390.1 (25), 270.1 (18), 167.1 (21), 149.0 (75), 105.1 (100), 77.1 (29). HRMS calcd for $\text{C}_{34}\text{H}_{21}\text{O}_4\text{F}$, 512.1420; found, 512.1424.

trans-(7R,8R)-bis(Benzoyloxy)-7,8-dihydro-2-fluorobenzo[a]pyrene (20). LRMS (70 eV): m/z (%) 512.2 (25, M^+), 270.1 (39), 122.1 (19), 105.1 (100), 71.1 (33). HRMS calcd for $\text{C}_{34}\text{H}_{21}\text{O}_4\text{F}$, 512.1424; found, 512.1428.

trans-(7S,8S)-Dihydroxy-7,8-dihydro-2-fluorobenzo[a]pyrene (19). To a solution of **18** (42 mg, 0.08 mmol) in THF (5 mL) was added sodium methoxide (0.6 mL, 0.5 M) in methanol. The reaction mixture was stirred under N_2 at room temperature for 30 min. The reaction was quenched by adding water, and the residual THF was removed under reduced pressure. The resulting aqueous layer was extracted with methylene chloride, and the combined organic extracts were washed with water and dried over anhydrous MgSO_4 . After solvent evaporation, the residue was purified with column chromatography on silica to afford the pure product **19** as a white solid (22.4 mg, 91%). ^1H NMR (CDCl_3): δ 8.56 (s, H_6 , 1H), 8.52 (d, $J_{11,12} = 9.4$ Hz, $\text{H}_{11,12}$, 2H), 8.11–8.22 (m, $\text{H}_{4,5}$, 2H), 8.00 (ddd, $J_{1,\text{F}} = 9.8$ Hz, $J_{1,3} = 1.8$ Hz, $J_{1,12} = 1.8$ Hz, $\text{H}_{1,3}$, 2H), 7.54 (dd, $J_{9,10} = 10.2$ Hz, $J_{8,10} = 2.2$ Hz, H_{10} , 1H), 6.33 (dd, $J_{9,10} = 10.1$ Hz, $J_{8,9} = 2.0$ Hz, H_9 , 1H), 5.10 (d, $J_{7,8} = 10.3$ Hz, H_7 , 1H), 4.61 (dd, $J_{7,8} = 10.3$ Hz, $J_{8,9} = 2.0$ Hz, H_8 , 1H). ^{13}C NMR (acetone- d_6): δ 161.71 (d, $J = 239.1$ Hz, C_2), 137.41, 135.72, 130.78, 130.40, 130.08, 129.53, 128.41, 127.95, 127.48, 126.52, 125.04, 124.72, 123.85, 123.23, 122.76, 111.94 (d, $J = 22.6$ Hz), 111.72 (d, $J = 22.3$ Hz), 76.32, 73.99. ^{19}F NMR (acetone- d_6): $\delta -111.45$ (apparent t, $^3J_{\text{H-F}} = 11.3, 7.5$ Hz). LRMS (70 eV): m/z (%) 304.2 (50, M^+), 286.2 (95), 257.2 (100), 233.2 (34), 168.1 (26), 128.8 (50), 115.1 (25). HRMS calcd for $\text{C}_{20}\text{H}_{13}\text{O}_2\text{F}$, 304.0904; found, 304.0900.

trans-(7R,8R)-Dihydroxy-7,8-dihydro-2-fluorobenzo[a]pyrene (21). LRMS (70 eV): m/z (%) 304.1 (16, M^+), 286.1 (100), 270.1 (73), 257.1 (79), 244.1 (14), 128.1 (18), 105.0 (10). HRMS calcd for $\text{C}_{20}\text{H}_{13}\text{O}_2\text{F}$, 304.0904; found, 304.0907.

trans-(7S,8R)-Dihydroxy-9R,10S-epoxy-7,8,9,10-tetrahydro-2-fluorobenzo[a]pyrene (23). To a solution of the dihydrodiol **19** (15.2 mg, 0.05 mmol) in dry THF (4 mL) was added an excess amount of freshly purified *meta*-chloroperbenzoic acid (mCPBA) (76 mg, 0.4 mmol). The reaction mixture was stirred at 0°C under N_2 for 20 min. The ice bath was removed, and the stirring was continued at room temperature for 40 min. The reaction mixture was diluted with ether, washed with iced water and 10% NaOH, and dried over anhydrous CaCO_3 . After filtration, the organic solvent was evaporated, and the residue was dried in a vacuum to obtain the diol epoxide product as a pale yellow solid (15 mg, 90%). ^1H NMR ($\text{DMSO}-d_6$): δ 8.81 (d, H_{11} , 1H), 8.67 (s, H_6 , 1H), 8.25 (m, 4H), 8.07 (d, 1H), 5.19 (d, $J = 4.4$ Hz, H_{10} , 1H), 4.97 (d, $J = 8.8$ Hz, H_7 , 1H), 4.07 (d, $J = 8.8$ Hz, H_8 , 1H), 3.93 (d, $J = 4.4$ Hz, H_9 , 1H). ^{19}F NMR (acetone- d_6): $\delta -116.60$ (apparent t, $^3J_{\text{H-F}} = 11.3, 7.5$ Hz). ESI-MS (negative mode): m/z (%) 319.19 (17), 301.18 (49), 283.36 (20), 255.32 (42), 227.28 (30), 172.15 (75), 157.17 (37), 143.15 (33), 135.12 (100). HRMS for $\text{M}^+ - \text{H}_2\text{O}$ ($\text{M}^+ - 18$) calcd for $\text{C}_{20}\text{H}_{11}\text{O}_2\text{F}$, 302.0743; found, 302.0740.

trans-(7R,8S)-Dihydroxy-9S,10R-epoxy-7,8,9,10-tetrahydro-2-fluorobenzo[a]pyrene (22). HRMS for $\text{M}^+ - \text{H}_2\text{O}$ ($\text{M}^+ - 18$) calcd for $\text{C}_{20}\text{H}_{11}\text{O}_2\text{F}$, 302.0743; found, 302.0741.

Diastereomeric Bis(menthoxyacetate) Esters of trans-(7S,8S)- and trans-(7R,8R)-Dihydroxy-7,8,9,10-tetrahydro-2-fluorobenzo[a]pyrene (17 and 16). Menthoxyacetylation reactions were carried out according to the literature procedures (33). To a solution of freshly prepared **12** (29 mg, 0.1 mmol, see above) in 1.5 mL of methylenechloride were added (–)-menthoxyacetyl chloride (44 μL), DMAP (1 mg), and pyridine (0.2 mL). The mixture was stirred under N_2 atmosphere at room temperature overnight. The mixture was diluted with ether, and the organic extracts were washed successively with water, 10% NaOH, and water and dried over anhydrous MgSO_4 . The solid residue obtained after evaporation was purified with silica column chromatography (hexane: $\text{CHCl}_3 = 1:1$) to give the menthoxyacetylated product **17** (63 mg, 90%). Enantiomeric excess was $>92\%$ according to HPLC integration (see

Figure 8b). Compound **17**: $^1\text{H NMR}$ (CDCl_3): δ 0.66, 2.03 (m, 34H), 2.40 (m, 1H), 2.49 (M, 1H), 3.08–3.42 (m, 2H), 3.57 (m, 2H), 4.03–4.22 (m, 4H), 5.48 (m, H_8 , 1H), 6.50 (d, $J = 5.4$ Hz, H_7 , 1H), 7.85 (m, $\text{H}_{1,3}$, 2H), 7.97 (m, 2H), 8.09 (d, 1H), 8.13 (s, H_6 , 1H), 8.29 (d, H_{11} , 1H). $^{13}\text{C NMR}$ (CDCl_3): δ 170.57, 170.24, 160.98 (d, $J = 244.0$ Hz, C_2), 133.48 (d, $J = 9.5$ Hz), 132.75 (d, $J = 9.2$ Hz), 131.21, 129.93, 129.36, 128.75, 127.97, 127.22 (d, $J = 3.5$ Hz), 126.73, 126.48 (d, $J = 3.7$ Hz), 124.43, 124.04, 121.51, 111.66 (d, $J = 23.0$ Hz), 111.07 (d, $J = 22.4$ Hz), 80.83, 80.57, 80.34, 71.49, 71.01, 60.45, 66.20, 66.09, 60.70, 48.20, 48.14, 40.23, 40.07, 34.47, 34.41, 31.55, 31.49, 25.57, 25.53, 24.41, 23.35, 22.89, 22.39, 20.96, 20.83, 16.32. Compound **16** was prepared in a similar manner from **14**. $^1\text{H NMR}$ (CDCl_3): δ 8.27 (d, H_{11} , 1H), 8.14 (s, H_6 , 1H), 8.09 (d, 1H), 7.95 (dd, 2H), 7.85 (m, $\text{H}_{1,3}$, 2H), 6.60 (d, H_7 , 1H), 5.49 (m, H_8 , 1H), 4.16 (m, 4H), 3.59 (m, 2H), 3.16 (m, 2H), 2.50–2.23 (m, 4H), 2.00 (dd, 2H), 1.62 (m, 4H), 1.27 (m, 6H), 1.04–0.69 (m, 22H). $^{13}\text{C NMR}$ (CDCl_3): δ 170.40, 170.19, 160.55 (d, $J = 244.7$ Hz, C_2), 133.36 (d, $J = 9.6$ Hz), 132.63 (d, $J = 9.6$ Hz), 131.12, 129.68, 129.25, 128.66, 127.87, 127.13 (d, $J = 3.9$ Hz), 126.80, 126.41 (d, $J = 3.5$ Hz), 124.30, 123.94, 121.37, 111.59 (d, $J = 22.8$ Hz), 111.00 (d, $J = 22.7$ Hz), 80.48, 80.31, 71.06, 70.76, 66.02, 65.79, 48.06, 48.02, 39.96, 39.87, 34.32, 31.45, 31.39, 29.69, 25.53, 25.43, 24.08, 23.27, 23.20, 22.61, 22.28, 22.19, 20.95, 20.85, 16.26, 16.20. Enantiomeric excess was >96% according to HPLC integration (see Figure 8a). A similar preparation was made for the racemic mixture and used for enantiomeric excess analyses (see Figure 8c).

Succinylation of 1-Fluoropyrene. 1-Fluoropyrene (220 mg, 1.0 mmol) (Supporting Information) was proportionally added to a mixture of anhydrous AlCl_3 (500) and succinic anhydride (120 mg, 1.2 mmol) in nitrobenzene (8 mL) at room temperature. The reaction proceeded and worked up as described above for succinylation of **6**. The crude solid containing a mixture of keto-acid derivatives was then treated with red phosphorus (100 mg) and HI (55%, 2.0 mL) in acetic acid (10 mL) and heated to reflux under N_2 for 2 days. The reduced acid was placed in HF solution in a closed Daiflon vessel and worked-up as described above for the cyclization of the 2-fluoro derivative. The crude mixture of dihydroarene was finally dehydrogenated with DDQ. HPLC analysis of the crude product indicated 68% 1-, 30% 3-, and 2% 6-fluorobenzo[*a*]pyrene (see Supporting Information, S1).

Synthesis of anti-FBP-Modified dG. A 0.5 mL solution of dGMP (50 mM, in 10 mM Tris-HCl buffer, pH 7.4) was added to 50 μL of anti-FBPDE (**22** or **23**, 1 mg/mL) in a 1:9 mixture of DMSO and acetonitrile, and the reaction was allowed to incubate at 37 °C for 20 h. Sep-Pak separation of the excess unmodified dGMP was conducted initially by eluting with water. The fractions containing *trans*-FBP- N^2 -dG adduct were eluted with 50% methanol and vacuum-dried. The residue was redissolved in 0.5 mL of Tris-HCl buffer (pH 9.0) containing 10 mM MgCl_2 and extracted with water-saturated ether to remove excess tetraols. The aqueous phase was then incubated for 3 h at 37 °C with 2.7 units of *Escherichia coli* alkaline phosphatase to remove the 5'-phosphate group. A pure adduct was obtained by a reverse phase HPLC (see Figure 10 for detailed HPLC conditions). Keeping the concentration of dGMP higher (around 50 mM) was critical as lower concentrations (5 mM) facilitate hydrolysis process. Also, the purity of FBPDE was a key factor for increasing the reaction efficiency and minimizing hydrolysis.

Synthesis of anti-FBP-Modified Oligodeoxynucleotides. Each oligodeoxynucleotide (100 μM , CCATXGCTACC where **X** = dC, dT) dissolved in 50 mM Tris-HCl and 5 mM EDTA (pH 7.5) was reacted with approximately 5-fold excess of either **22** or **23** freshly prepared in ~10% DMSO. The reaction mixture was kept on ice in darkness overnight. The hydrolyzed tetraols were removed by extensive extraction with buffer-saturated ethyl acetate. Modified oligonucleotide adducts were purified using a reverse phase HPLC (see Figure 12 for detailed HPLC conditions).

Enzymatic Digestion of FBP-Modified Oligodeoxynucleotides. Approximately 2 μmol of the FBP-modified oligomers were dissolved in 3 mL of Bis-Tris-EDTA (pH 7.0) buffer containing 0.5 mg of

DNase I and incubated at 37 °C with shaking for 3–4 h. Subsequently, snake venom phosphodiesterase I (100 μL , 1 unit/2 mL, 0.05 units) and 50–100 μL of alkaline phosphatase (100 units/2 mL, 2.5 units) were added into the mixture, which was incubated at 37 °C with shaking for 16 h. The mixture was extracted with butanol three times. The combined butanol extracts were back-washed with water and concentrated using a SpeedVac. The residue was reconstituted in 0.5 mL of methanol for HPLC analysis. Unmodified oligomers were digested similarly to serve as controls (see Figure 13 for detailed HPLC conditions).

Hydrolysis of 2-FBPDE to Tetraols. To a mixture of 50% acetone–water (50 mL) was added 29 mg of **22** or **23** in 5 mL of THF. After agitation at 37 °C overnight, tetraols were extracted into ethyl acetate and separated by reverse phase HPLC using Beckman Ultrasphere ODS (4.6 mm \times 250 mm) with a flow rate of 1.0 mL/min. Gradient conditions were 50% methanol in water for 10 min, followed by a linear gradient that increased the methanol composition by 1% per minute for 35 min.

RSRS-*trans*-anti-FBPT. $^1\text{H NMR}$ (acetone- d_6): δ 4.34 (dd, $J_{8,9} = 1.9$ Hz, $J_{7,8} = 8.8$ Hz, H_8 , 1H), 4.49 (dd, $J_{9,10} = 3.2$ Hz, $J_{8,9} = 1.9$ Hz, H_9 , 1H), 5.21 (d, $J_{7,8} = 8.8$ Hz, H_7 , 1H), 5.71 (d, $J_{9,10} = 3.3$ Hz, H_{10} , 1H), 8.00–8.07 (m, $\text{H}_{1,3}$, 2H), 8.14 (d, $J_{4,5} = 9.0$ Hz, 1H), 8.23 (d, $J_{4,5} = 9.0$ Hz, 1H), 8.25 (d, $J_{11,12} = 9.3$ Hz, H_{12} , 1H), 8.58 (s, H_6 , 1H), 8.67 (d, $J_{11,12} = 9.3$ Hz, H_{11} , 1H). LRMS (70 eV): m/z (%) 338.2 (98, M^+), 286.2 (100), 273.2 (91), 257.2 (84), 244.2 (46), 232.2 (57), 220.2 (76), 199.2 (47), 184.2 (23), 168.2 (46), 139.1 (42), 128.0 (50), 115.1 (53), 77.1 (91). HRMS calcd for $\text{C}_{20}\text{H}_{15}\text{O}_4\text{F}$, 338.0954; found, 338.0951.

Results

Synthesis. It was our aim to generate fluoro-BPDEs that were structurally and conformationally analogous to BPDE. Achieving this goal required that fluorine be added at positions (i.e., C1, -2, or -3) that are situated away from the diol epoxide moiety. Indeed, it has been shown that substitution of fluorine at the sterically hindered position 6 alters the BP-7,8-diol conformation significantly (15, 16).

Initially, we pursued preparation of 1-fluoro-BPDE because of the ready availability of 1-fluoropyrene as a starting building block. Friedel–Crafts succinylation of 1-fluoropyrene, however, produced a mixture of keto-acid intermediates that were difficult to separate (Figure 2). The crude mixture was converted into fully aromatic fluorobenzo[*a*]pyrenes by a series of reactions involving keto reduction (HI/P) and cyclization (HF), followed by aromatization ($\text{NaBH}_4/p\text{-TsOH}/2,3\text{-dichloro-5,6-dicyano-1,4-benzoquinone}$) (DDQ) (Figure 2) (5). The HPLC profile of the final product showed that it consisted of 68% ($R_t = 18.3$ min) 3-fluorobenzo[*a*]pyrene, 30% ($R_t = 21.6$ min) 1-fluorobenzo[*a*]pyrene, and 2% of the 6-fluoro isomer ($R_t = 26.6$ min) (Supporting Information, S1). These compounds were identified by comparison of retention times and the UV and $^1\text{H NMR}$ properties of independently prepared standard samples (17, 18). The UV absorption profiles of the three isomers were generally similar except that the 6-fluoro isomer exhibited a significant red shift of absorptions centered on 280 nm (Supporting Information, S1). This result indicates that the electronic effect of fluorine substitution at position 6 is different from that at positions 1 and 3. Clearly, the regioselectivity of succinylation in the product prepared from 1-fluoropyrene is an issue.

Figure 2 shows all possible succinylation pathways and the anticipated cyclization product that was generated from 1-fluoropyrene. For example, reactions at the most electrophilic positions 6 and 8 would produce 3- or 1-fluorobenzo[*a*]pyrene, respectively, whereas reaction at position 7 could give either product depending on the direction of ring closure. Reactions at the 2 and 3 positions are predicted to produce 6-fluorobenzo-

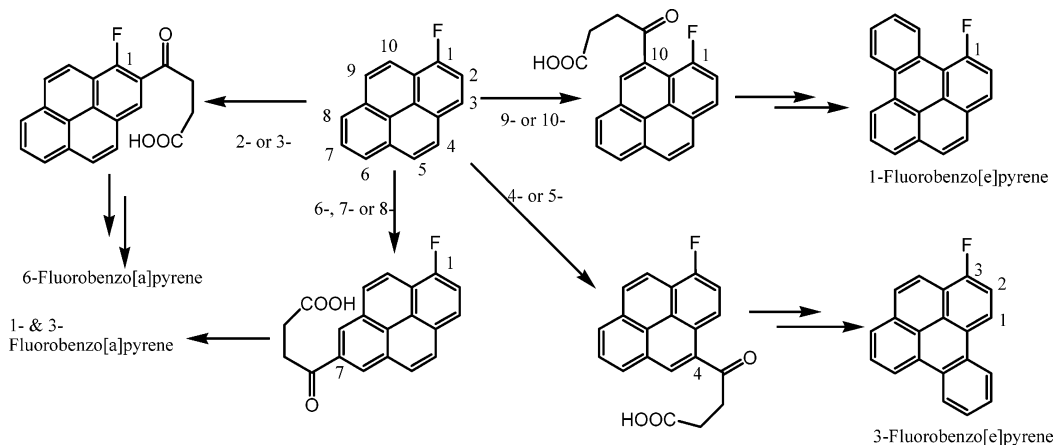


Figure 2. Possible fluoro compounds derived from succinylation of 1-fluoropyrene and subsequent aromatization reaction.

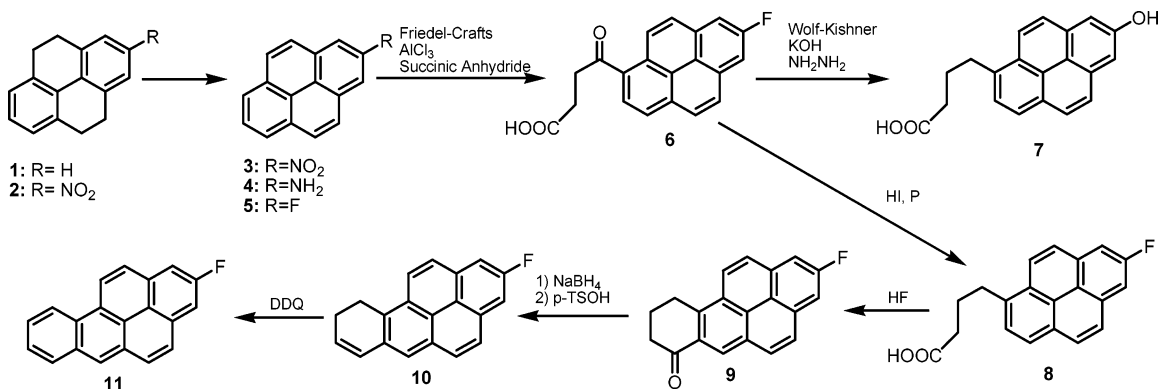


Figure 3. Synthesis of 2-fluorobenzo[a]pyrene and 9,10-dihydro-2-fluorobenzo[a]pyrene (10).

[a]pyrene, which turned out to be a minor pathway (2%). Similar reactions at positions 4, 5 or 9, 10 should produce 3- or 1-fluorobenzo[e]pyrene, respectively; however, such products were not detected.

2-Fluoro-9,10-dihydrobenzo[a]pyrene. Observing the disadvantages inherent in preparing 1-FBPDE, we proceeded to turn our attention to 2-fluoropyrene as a starting material (Figure 3). The symmetrical nature of 2-fluoropyrene should result in succinylation reactions (5) at position 6 or 8, which upon cyclization would provide the desired 2-fluorobenzo[a]pyrene moiety. The succinylation reaction of 2-fluoropyrene indeed led exclusively to keto-acid 6 (Figure 3). Direct fluorination of the commercially available pyrene has been reported but resulted in a mixture of 1-, 2-, and 4-isomers (19). The most efficient route for a gram scale preparation of 2-fluoropyrene (5) was the Balz–Schiemann reaction [*t*-BuONO/(Et₂O)BF₃] of 2-aminopyrene (4), which can be attained by either NaNH₂ treatment of 1-bromopyrene (20) or nitration of 4,5,9,10-tetrahydropyrene (21–24), followed by aromatization and reduction (1 → 4) (25, 26) (Supporting Information).

The keto-reduction of 6 by the Wolf–Kishner reaction (NH₂NH₂/KOH) resulted in the phenolic 7 as the sole product. LRMS of 7 indicated that there was a molecular ion present at *m/z* 304, instead at the anticipated *m/z* 306 for the acid product 8. No signal was observed in ¹⁹F NMR. In addition, no H–F couplings were observed for the H1 and H3 protons in ¹H NMR (S12). The decoupled ¹³C NMR spectrum of 7 showed a singlet at 150.6 ppm instead of the characteristic coupled fluorine doublet in that region (S13). These results are consistent with the presence of phenol functionality at position C2 (S13). The harsh basic Wolf–Kishner conditions appear to be responsible for the loss of the fluorine atom. The desired keto reduction,

however, occurred under mild conditions involving HI/P (5, 27). The acid product 8 was thoroughly characterized by ¹H and ¹³C NMR and mass spectrometry. The decoupled ¹³C NMR spectrum displayed a doublet at 160.3 ppm (¹J_{C2–F2} = 242 Hz), which corresponds to C2 (S12). In fact, this doublet carbon signal was used as an important indicator for the presence of fluorine at C2 throughout the synthesis. Cyclization of 8 took place readily in HF at room temperature to produce the 7-keto derivative 9 in a nearly quantitative yield. Transformation of 9 to the dihydroarene 10, a key synthetic intermediate, was carried out by the commonly employed reduction/dehydration (NaBH₄/p-TsOH) procedure (5, 28, 29). Subsequent dehydrogenation of 10 with DDQ in refluxing benzene yielded 2-fluorobenzo[a]pyrene (11).

trans-7*S*,8*S*- (or 7*R*,8*R*)-Dihydroxy-7,8,9,10-tetrahydro-2-fluorobenzo[a]pyrene. Stereoselective transformation of 10 to the target chiral diol epoxides was achieved via the general procedures of Harvey et al. (30) and Harris et al. (31), who independently demonstrated the utility of Jacobsen catalysts (32) for preparation of enantiomeric (+)-*RSSR*- and (–)-*SRRS*-anti-BPDEs. Treatment of 10 with NaOCl in the presence of (*R,R*)-*N,N'*-bis(3,5-di-*tert*-butylsalicylidene)-1,2-cyclohexanediaminomanganese(III) chloride generated the 7*R*,8*S* epoxide (not shown). Treatment of the crude epoxide with 10-camphorsulfonic acid (10-CSA) in acetone/water produced exclusively the *trans*-7*S*,8*S*-tetrahydrodiol 12 (Figure 4). The enantiomeric excess of the tetrahydrodiol was greater than 92% as determined by HPLC analysis of its diastereomeric bis-(–)-menthoxyacetate (see below) (33). A similar reaction sequence with the *S,S*-Jacobsen catalyst generated in the corresponding 7*R*,8*R*-tetrahydrodiol 14 with greater than 96% enantiomeric excess.

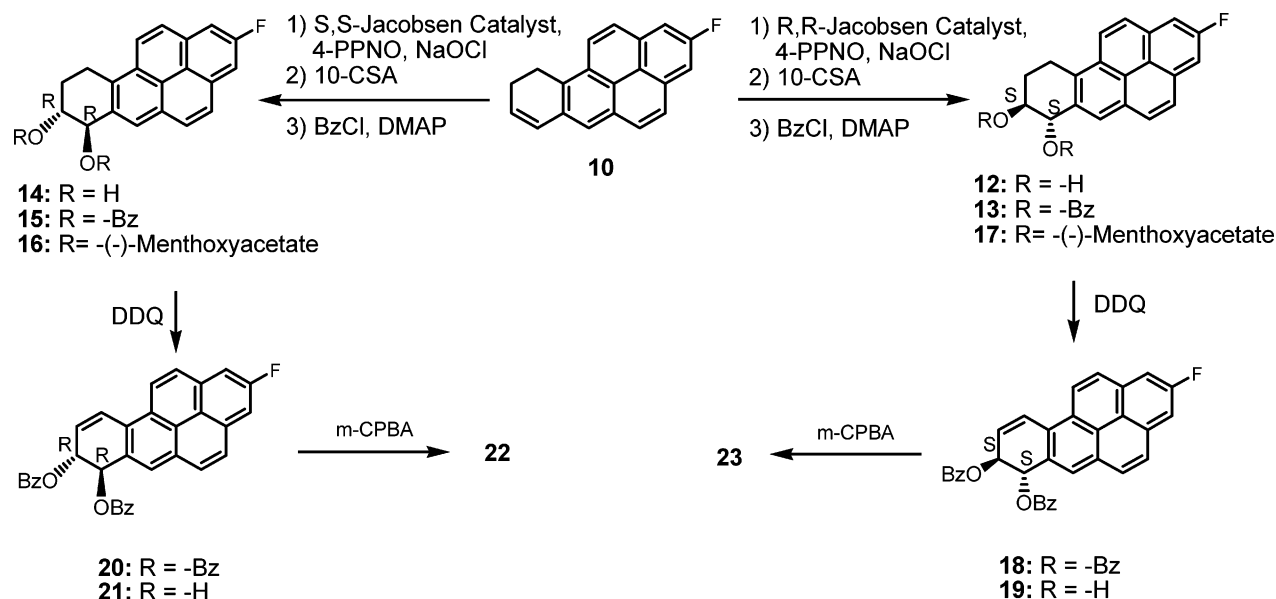


Figure 4. Stereospecific syntheses of **22** and **23** via a dihydroarene method using Jacobsen catalysts. 4-PPNO, 4-phenylpyridine N-oxide; 10-CSA, 10-camphorsulfonic acid.

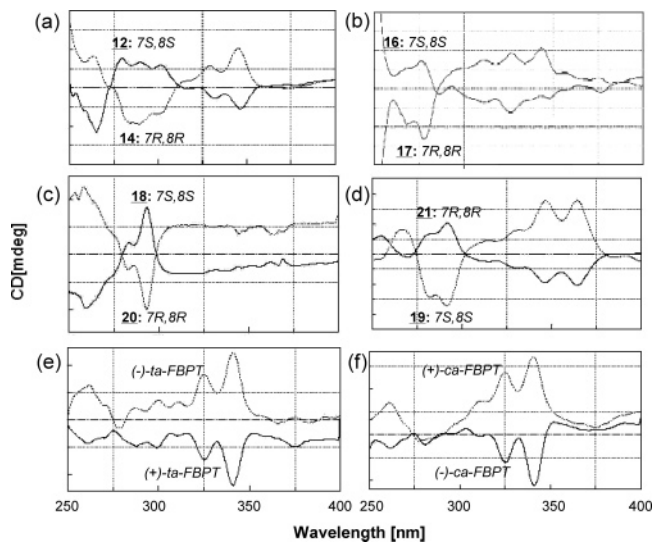


Figure 5. CD spectra of 2-fluorobenzo[*a*]pyrenyl derivatives (a–d) and tetraols (e and f) in enantiomeric pairs. See Figure 4 for structures. ta, trans-anti; ca, cis-anti.

Absolute configurations of the tetrahydrodiols were determined by comparative CD spectral analysis with the corresponding BP derivatives. As shown in Figure 5a, the CD spectrum of 7*S*,8*S*-tetrahydrodiol **12** exhibited multiple positive and negative ellipticities in the ~270–310 and ~310–360 nm ranges, respectively. A mirror image of the CD spectrum of **12** was observed for the 7*R*,8*R*-enantiomer **14**. The CD spectrum of **14** closely matched that of the BP counterpart (33–35), which was expected since the isosteric fluorine substitution at C2 is unlikely to alter the CD significantly. Figure 5b shows the CD spectra of the bis-(–)-menthoxyacetates **16** and **17**. The widened CD pattern in the 280–380 nm range may arise from the strong longitudinal interaction between the two menthoxyacetate groups and the pyrenyl ring system (34). Despite their diastereomeric relationship, the CD patterns of **16** and **17** were essentially mirror images of each other.

trans-7*S*,8*S*- (or 7*R*,8*R*)-Dihydroxy-7,8-dihydro-2-fluorobenzo[*a*]pyrene. A benzylation of **12** produced the *trans*-tetrahydrodibenzoate **13** (Figure 4) (5, 28, 29). Dehydrogenation of **13** with DDQ in refluxing dry benzene resulted in the *trans*-

7*S*,8*S*-dihydro-dibenzoate **18** with an excellent yield (91%). A similar reaction sequence involving **14** produced the corresponding 7*R*,8*R*-isomer **20** via **15**. The structures of **18** and **20** were characterized thoroughly by HRMS, NMR (¹H, ¹³C, and ¹⁹F), CD, and elemental analyses. Figure 5c shows the mirror CD images of the enantiomeric pairs (**18/20**). The strong intensities of the signals at ~260 and ~95 nm relative to those above 300 nm may be due to the strong coupling between the two dibenzoyl groups (34).

Methanolysis of **18** and **20** with sodium methoxide in methanol and THF produced the *trans*-dihydrodiols **19** and **21**, respectively. As shown in Figure 5d, the overall CD patterns of the dihydrodiols were completely opposite from that of the tetrahydrodiols **12/14** (Figure 5a). A similar CD switch has been observed between the tetrahydro and the dihydro 7*R*,8*R*-BP-diol sequence (34). The intense ellipticities observed in the 300–380 nm region arise from the stronger longitudinal transitions, clearly reflecting the contribution of the extended π -electron conjugation (C_{9,10}) to the pyrene ring system. The CD spectrum of **21** was essentially identical to that of *trans*-BP-7*R*,8*R*-dihydrodiol (33–35). Furthermore, the ¹H NMR coupling constant (³*J*_{7,8}) between H7 (5.10 ppm) and H8 (4.61 ppm) of **21** is ~10 Hz, which is similar to that observed for the nonfluoro counterpart BP-7,8-dihydrodiol (36). Taken together, these results indicate that **21** preferentially adopts a pseudo-diequatorial conformation.

trans-7*R*,8*S*-Dihydroxy-9*S*,10*R*- (or *trans*-7*S*,8*R*-Dihydroxy-9*R*,10*S*)-epoxy-7,8,9,10-tetrahydro-2-fluorobenzo[*a*]pyrene (22** and **23**).** The target *anti*-diol epoxides (**22** and **23**) were prepared by reacting the dihydrodiols (**19** or **21**) with an excess amount of mCPBA in dry THF according to previously described protocols (37–41). The ESI-MS spectrum (Supporting Information, S38) of *anti*-FBPDE in the negative ion mode exhibited a [M – H][–] ion at *m/z* 319. The fragments at *m/z* 301 and 283 are a result of the loss of one or two H₂O molecules, respectively.

Figure 6 shows the ¹H NMR spectrum of **23** in acetone-*d*₆. The spectral pattern is similar to that recorded for the racemic *anti*-BPDE (37–41), except for the upfield aromatic region. The most shielded aromatic signal at 8.07 ppm showed a clean doublet with the integration of two protons and a large H–F

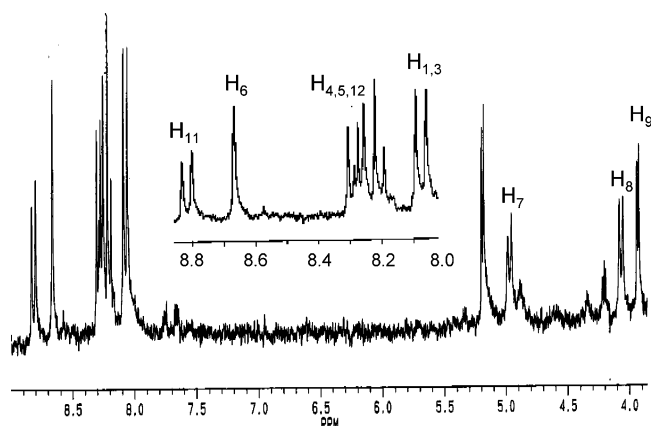


Figure 6. ^1H NMR spectrum of **23** in acetone- d_6 . The inset shows the expanded aromatic region.

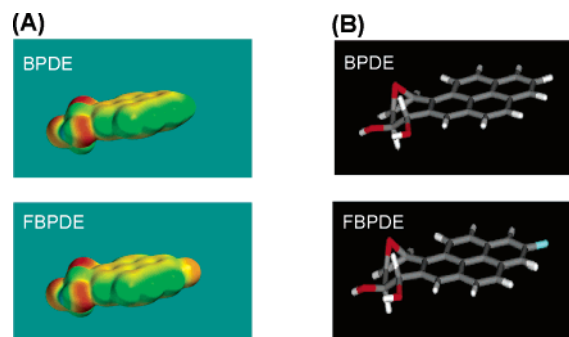


Figure 7. (A) Electrostatic and (B) stick presentations of (–)-(7*S*,8*R*,9*R*,10*S*)-anti-BPDE (top) and (–)-(7*S*,8*R*,9*R*,10*S*)-anti-FBPDE (**23**) (bottom). Colors in the electrostatic map are assigned according to the potentials: red (most negative) < orange < yellow < green < blue (most positive). See Figure 1 for structures.

coupling ($^3J_{\text{HF}} = 11.3$ Hz) and thus assigned as H1,3. As expected, the bay region H₁₁ doublet and H₆ singlet were the most deshielded. The $^3J_{7,8}$ vicinal coupling constant of a diol epoxide serves as a convenient indicator of the diol conformation (5, 36). In general, anti-BPDEs showed a $^3J_{7,8}$ value in the range of 8.25–9.0 Hz, which is typical for a molecule with a diequatorial conformation (36). This is contrasted to the smaller $^3J_{7,8}$ couplings observed for syn-BPDE (6.0 Hz) (36) or anti-6-fluoro-BPDE (5.5 Hz) (16), which are thought to exist mainly in a diaxial conformation. The conformational effect observed for the latter is likely caused by an unfavorable electrostatic interaction between the fluorine at C6 and the neighboring hydroxyl group such that the hydroxyl groups have a greater preference for an axial orientation. The $J_{7,8}$ coupling of anti-FBPDE was determined to be 8.8 Hz in acetone- d_6 , which indicates its preference for pseudo-diequatorial conformation. This conclusion was supported by the DFT B3LYP/6-31G* calculations (42) of BPDE and FBPDE. As shown in Figure 7, the presence of C2-fluorine in FBPDE had little impact on the overall electronic charge density of the molecule, especially for the 7,8-dihydrodiol-9,10-epoxide moiety.

Enantiomeric Excess Analysis. In accordance with published procedures (33), each of the crude chiral tetrahydrodiols (**12** and **14**) was reacted with (–)-menthoxyacetyl chloride to produce diastereomeric adducts. Figure 8a,b shows the normal phase HPLC chromatograms of the resulting di-(–)-menthoxyacetates, which were compared with that (Figure 8c) of a racemic mixture derived from a similar reaction in the absence of Jacobsen catalyst. The peaks at 40 and 48 min represent 7*R*,8*R*- and 7*S*,8*S*-di-(–)-menthoxyacetates, respectively. Area integration calculations determined that the enantiomeric excess

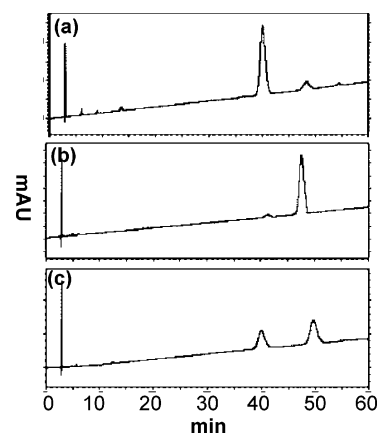


Figure 8. HPLC profiles of bis-(–)-menthoxyacetate esters of (a) 7*R*,8*R*- and (b) 7*S*,8*S*-*trans*-7,8,9,10-tetrahydro-2-fluorobenzo[*a*]pyrene; (c) control: a racemic bis-(–)-menthoxyacetate obtained from a reaction without Jacobsen catalyst. HPLC conditions: Beckman Ultrasphere Si column (4.6 mm × 250 mm), 100% methylene chloride isocratic, 1 mL/min.

of the diols with the *R,R*- and *S,S*-Jacobsen catalyst were greater than 92 and 96%, respectively. The diastereomeric di-(–)-menthoxyacetates were also purified and characterized by NMR, MS, and CD.

Hydrolysis of anti-FBPDE to Tetraols. The enantiomeric anti-FBPDEs (**22** and **23**) were readily hydrolyzed in an aqueous solution to produce the tetraols, FBPTs. For each enantiomeric anti-FBPDE, two FBPTs are formed depending on the nature (*trans* or *cis*) of the epoxide ring opening (Figure 9). The HPLC profiles (Supporting Information, S34) of the FBPTs derived from hydrolysis of **22** showed the early ($R_t = 17$ min) and late ($R_t = 21$ min) eluting peaks in a ratio of ~9:1. A similar set of FBPTs was obtained from the hydrolysis of **23**. Negative ion mode ESI-TOF-MS of all four FBPT isomers gave peaks at m/z 337 and 319, which correspond to $[\text{M} - \text{H}]^-$ and $[\text{M} - \text{H} - \text{H}_2\text{O}]^-$, respectively. In general, the vicinal $^3J_{7,8}$ coupling constants for *trans*-tetraols from anti-BPDE have been shown to be significantly larger (~9 Hz) than the *cis*-tetraols (~4 Hz) (38). The early eluting major peak in each case gave larger $^3J_{7,8}$ values than the late eluting minor isomer (Table 1) and therefore was designated as the *trans*-tetraol. This designation scheme was supported by CD data. According to the hydrolysis scheme shown in Figure 9, the two early eluting major fractions corresponded to an enantiomeric pair: *RSRS*- and *SRSR-trans*-anti-FBPT. A similar pair was derived from the two late eluting fractions: *RSRR*- and *SRSS-cis*-anti-FBPT. As expected, the CD spectra of the two enantiomeric FBPT pairs were mirror images of each other (Figure 5e,f).

FBP-Modified N²-dG. As in the case of hydrolysis, reactions of each enantiomeric anti-FBPDE with dGMP were expected to produce a *trans*- or a *cis*-N²-dG adduct, depending on the nature of the epoxide opening (Figure 9) (43–46). Although a dephosphorylation step is required in isolating the adducts, use of dGMP at higher concentrations instead of dG has shown to be advantageous in producing adducts in greater yields with better regioselectivity (43, 44). Figure 10 shows a typical HPLC chromatogram and the on-line UV analyses of the reaction components obtained from the reaction of **22** with dGMP in Tris buffer at 37 °C and subsequent treatment with alkaline phosphatase. The major adduct fraction at 40.5 min was isolated for both MS and CD spectral characterization. The ESI-TOF-MS spectrum of the fraction in positive ion mode exhibited signals at m/z 587 and 471, which correspond to $[\text{M} + \text{H}]^+$ and $[\text{M} + \text{H} - \text{sugar}]^+$, respectively. A similar reaction was

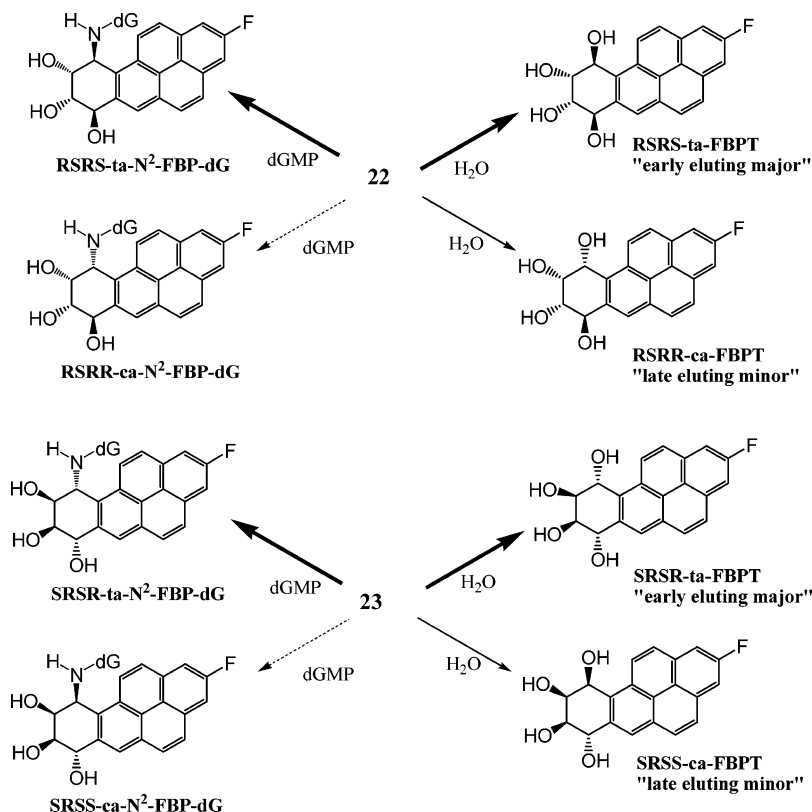


Figure 9. Reactions of **22** and **23** with H₂O and dGMP. ta, trans-anti; ca, cis-anti.

Table 1. Key Coupling Constants of Tetraols from *RSSR-anti-FBPDE* (**22**)

	$J_{7,8}$ (Hz) ^b	$J_{8,9}$ (Hz) ^b	$J_{9,10}$ (Hz) ^b
<i>RRSR-trans-anti-FBPT</i> ^a	8.8 (9.3)	1.9 (2.4)	3.2 (3.7)
<i>RSRR-cis-anti-FBPT</i> ^a	4.2 (4.2)	2.2 (2.6)	4.9 (4.3)

^a See Figure 9 for structures. ^b Data in parentheses are taken from ref 16 and represent the tetraols from the corresponding (+)-*anti*-BPDE.

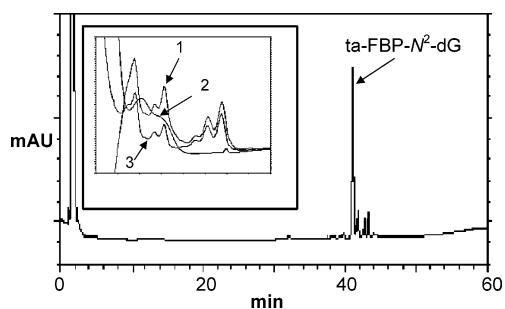


Figure 10. HPLC profile of the mixture obtained from a reaction of **22** with dGMP, followed by treatment with alkaline phosphatase. The inset shows UV spectra of *RRSR-trans-anti-FBP-N*²-dG (1), dG (2), *RSRR-anti-FBPDE* (**22**) (3). HPLC conditions: Phenomenox Luna 5 μ m C₁₈ (150 mm \times 4.6 mm) preheated at 40 °C with a flow rate of 1.0 mL/min. The mobile phase consisted of 10.0 mM ammonium acetate, pH 7.0 (solvent A), and a 1:1 mixture of solvent A with acetonitrile (solvent B). Gradient conditions were 1% B in A (5 min); 1–10% B in A (8 min); 10–20% B in A (10 min); and 20–60% B in A (38 min) at a flow rate of 2 mL/min.

also performed for **23**, and the major fraction gave similar MS characteristics. We were unable to isolate a sufficient material for ¹H NMR experiments.

Figure 11 shows that the CD spectra of the major fractions are virtually mirror images of each other despite the fact that they are diastereomeric to each other. The observed CD profiles are matched well with those derived from the corresponding (+)- and (–)-*anti*-BPDE, thus supporting their absolute con-

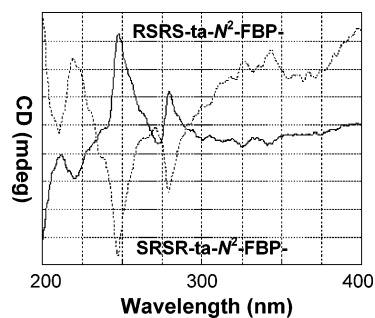


Figure 11. CD spectra of *RRSR-trans-anti-FBP-N*²-dG (—) and *SRSR-trans-anti-FBP-N*²-dG (---). ta, trans-anti.

figurations (47, 48). The *RRSR-trans-anti-N*²-dG adduct has a 10*S* as the absolute configuration at the benzylic carbon, which exhibits a strong positive band at 248 nm. The *SRSR-trans* adduct has a 10*R* as the absolute configuration and shows a negative band at the same wavelength (8). Taken together, these results indicate that the major fraction in each case was the *trans-N*²-dG adduct and that C2-fluorine substitution did not perturb the overall chiral conformation of the BP-*N*²-dG adduct.

FBP-Modified Oligodeoxynucleotides. Reactions of each of **22** and **23** with 11-mer oligodeoxynucleotides (Figure 1b, 5'-CCATXGCTACC-3' where X = dT, oligo I; X = dC, oligo II) were carried out in parallel experiments. We were able to isolate the single major fractions for each reaction, except for **23-anti**-oligo I. The base sequence contexts of the oligonucleotides used in this experiment were identical to those employed in the previously described CD and UV melting studies of the four major BPDE-modified adducts (S1). Figure 12a shows a typical HPLC chromatogram obtained from reaction of **22** with oligo II. On the basis of online UV analyses, the small HPLC peak at 9.8 min was identified as being the signature of the modified oligonucleotide and the tall peak at 27.0 min as that of *RRSR-ta-FBPT* (Figure 9). The HPLC profile of the purified oligomer

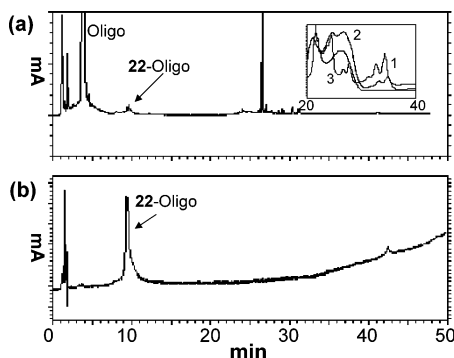


Figure 12. HPLC chromatograms of (a) the mixture obtained from a reaction of **22** with oligo II (5'-CCATCGCTACC-3') and (b) the fraction containing the modified oligonucleotide. The inset in panel a shows the UV spectra of **22** (1), FBP-modified oligo II (2), and unmodified oligo II (3). HPLC conditions: Waters XTerra MS C₁₈ 2.5 μ m, 10 mm \times 50 mm preheated at 40 $^{\circ}$ C. The mobile systems were the same as those used for separation of the N²-dG adduct (Figure 12): 10–20% of B in A (10 min); isocratic 20% of B in A (10 min); 20–30% of B in A (10 min); 30–60% of B in A (30 min); and 60% of B in A (20 min) at a flow rate of 2 mL/min.

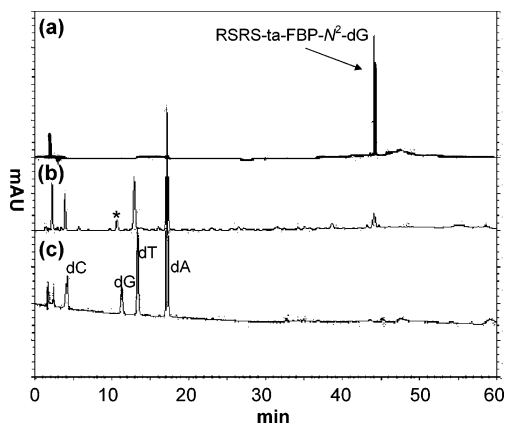


Figure 13. HPLC chromatograms of (a) the standard RSRS-trans-anti-FBP-N²-dG, enzyme-digested mixtures derived from (b) **22**-anti-FBPDE-modified duplex II (* denotes impurity), and (c) unmodified oligo II. HPLC conditions: Waters XTerra MS C₁₈ 2.5 μ m, 10 mm \times 50 mm. The mobile systems were the same as in Figure 12. Gradient conditions were 1% of B in A (5 min); 1–10% of B in A (8 min); 10–20% of B in A (10 min); and 20–60% of B in A (38 min) at a flow rate of 2 mL/min.

adduct is shown in Figure 12b. Figure 13 shows the HPLC chromatograms of the standard RSRS-*ta*-N²-FBP-dG adduct, the enzyme digests derived from **22**-FBP-oligo II, and the unmodified control. All of these were performed under the same conditions. The digest from the modified oligo II (Figure 13b) produced no dG, although a new and highly hydrophobic peak at 44 min, which coeluted with the standard RSRS-*ta*-FBP-N²-dG adduct (Figure 13a), was observed. This result confirmed that the single dG in the oligonucleotide was modified by reaction with FBPDE.

ESI-TOF mass spectra of the two FBP-oligo I adducts (MW = 3571) exhibited fragments at m/z 1785.5 and 1189.3, which correspond to the double and triple charged species, respectively. Similarly, FBP-modified oligo II adducts (MW = 3556) displayed the double and triple charged fragments at m/z 1777 and 1184, respectively. Other modified oligonucleotides were characterized similarly (Supporting Information, S2, S3, and S41).

CD of FBP-Modified Oligonucleotide Duplexes. The three anti-FBP-modified oligonucleotides described above were annealed with the appropriate sequences to form fully comple-

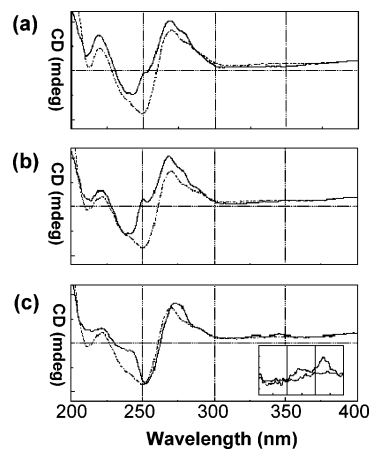


Figure 14. Comparison of the CD spectra of FBP-modified (—) and control (---) duplexes: (a) **22**-*trans*-FBP-duplex I, (b) **22**-*trans*-FBP-duplex II, and (c) **23**-*trans*-FBP-duplex II (inset, 300–360 nm).

mentary duplexes. Figure 14 shows the CD spectra of **22**-modified duplexes I and II as well as **23**-modified duplex II. The unmodified duplexes (dotted lines) are included for comparison. As expected for a B-form DNA duplex, the modified duplexes exhibited distinct positive and negative CD bands at around \sim 270 and \sim 240 nm, respectively (8, 47, 48). The low intensity signals observed in the 300–350 nm range for the modified duplexes were characteristic for an induced CD (ICD) of a pyrene chromophore intercalated with a DNA helix (49, 50). Despite sequence differences, **22**-modified duplexes I and II (Figure 14a,b) exhibited strikingly similar CD spectra patterns. The major CD bands were shifted to shorter wavelengths in going from the unmodified to the modified. Unlike **22**-duplex II (Figure 14b), the major CD bands of **23**-duplex II (Figure 14c) were shifted slightly to longer wavelengths relative to the control. The **22**-duplexes I and II showed slightly negative ICD, whereas **23**-duplex II exhibited relatively strong positive ICD in the 300–350 nm range (Figure 14c, inset). Pradhan et al. (49, 50) have indicated the latter as evidence for the minor groove conformation with 3'-orientation of BP. They have shown that the magnitude of BP-based ICD is dependent upon the sequence context and the particular adduct isomers studied. For example, the low intensity negative ICD observed for **22**-duplex I might indicate the prevalence of conformational heterogeneity. The shapes and signs of the observed ICD are in excellent agreement with data previously reported by Arghavani et al. (51) for studies of identical sequence contexts modified by either (+)- and (–)-anti-BPDE.

Figure 15 shows temperature-dependent CD spectra of the three FBP-modified duplexes (15 \sim 85 $^{\circ}$ C) discussed above. As expected, the intensities of the 275 and 240 nm CD bands decreased as temperatures increase. Increasing temperatures above 45 $^{\circ}$ C resulted in the formation of distinctive isosbestic points with the effects being greater for the duplexes modified with **22** (Figure 15a,b). Such effects were not observed for **23**-duplex II (Figure 15c) and the corresponding unmodified duplexes (not shown). The heterogeneous CD patterns observed at higher temperatures must arise from an increasing content of single strand conformation. These results indicate that the conformational dynamics of BP-modified duplexes during helix-coil transition are complicated due the presence of conformational heterogeneity (minor groove and intercalated conformers).

UV Melting Experiments. The 11-mer complementary duplexes used in the CD studies were also used for UV melting experiments. The thermodynamic parameters were calculated

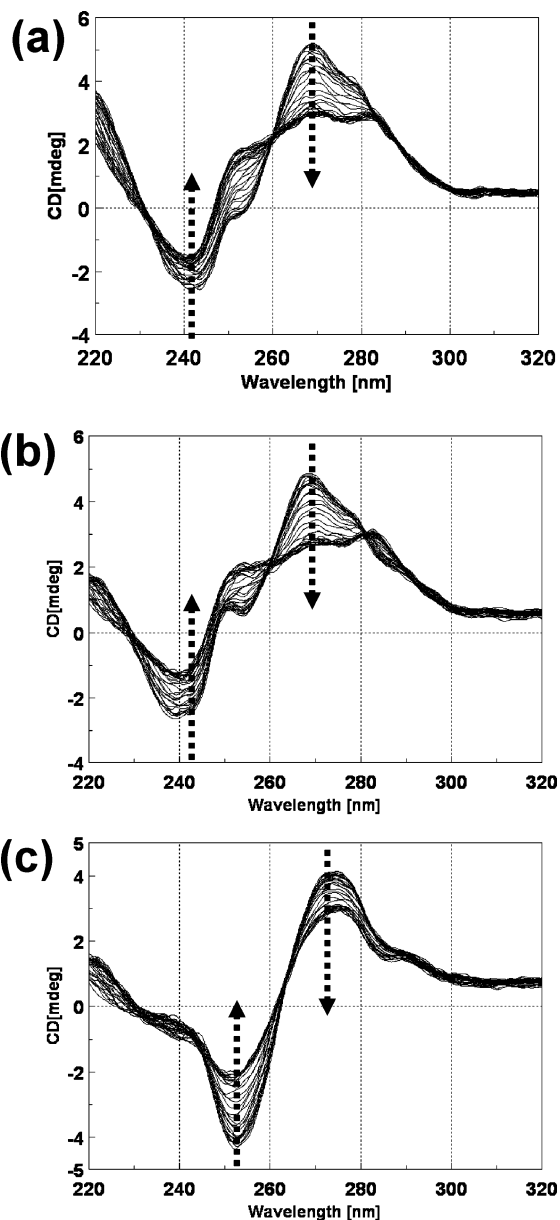


Figure 15. Temperature-dependent CD spectra for (a) **22-trans**-FBP-duplex I, (b) **22-trans**-FBP-duplex II, and (c) **23-trans**-FBP-duplex II. Dotted arrows denote increases in temperature (15 → 85 °C for every 5 °C).

Table 2. Thermodynamic Parameters of Duplex Formation and the Effect of Carcinogen Modification

duplex ^a	$-\Delta G^\circ$ ^b (kcal/mol)	$\Delta\Delta G^\circ$ ^b (kcal/mol)	T_m ^b (°C)	ΔT_m ^b (°C)
unmodified duplex I	11.0 (12.2) ^c		53.7 (59.7)	
unmodified duplex II	11.7 (13.4)		60.1 (63.9)	
22-trans -FBP-I	8.4 (9.3)	2.6 (2.9)	44.9 (51.2)	8.8 (8.5)
22-trans -FBP-II	9.4 (10.3)	2.3 (3.1)	53.0 (55.7)	7.1 (8.2)
23-trans -FBP-II	10.0 (11.0)	1.7 (2.4)	56.3 (59.0)	3.8 (4.9)

^a Duplex I, (5'-CCATTG*CTACC-3')(5'-GGTAGCAATGG-3'); duplex II, (5'-CCATCG*CTACC-3')(5'-GGTAGCGATGG-3'). ^b Measured in 0.2 M NaCl. The average standard deviations for $-\Delta G^\circ$, $-\Delta H^\circ$, and $-\Delta S^\circ$ are ± 0.2 , ± 6.3 , and ± 19.2 , respectively. ^c Data in parentheses are taken from ref 51 and represent the corresponding BPDE-modified duplexes in 1.0 M NaCl; calculated from 10^{-4} M duplex concentration.

using the MELTWIN Program, and the results are summarized in Table 2. The effects of FBP modification were examined by comparison of the $-\Delta G^\circ$ and T_m values calculated from the FBPDE-modified duplexes (this study, 0.2 M NaCl) with those

(shown in parentheses, 1.0 M NaCl) reported by Arghavani et al. (51) who have used identical sequence contexts to investigate the UV melting properties of four BPDE-modified duplexes. The consistently lower values observed for the FBP-modified duplexes are probably due to the lower salt conditions (0.2 M NaCl) employed in the present study. Nevertheless, both the controls and the FBPDE-modified duplexes exhibited UV melting profiles that are characteristic of a monophasic sigmoidal two-state helix-coil transition (not shown). Basically, the FBPDE modification resulted in a reduced T_m and $-\Delta G^\circ$. The decreases in T_m indicate that the covalent binding of the *anti*-FBPDE with the central dG residue leads to destabilization of the duplex. Duplex II, unmodified or modified, exhibited higher T_m and $-\Delta G^\circ$ values than did duplex I, which has a dT on the immediate 5'-end of the modified dG. Similar $\Delta\Delta G^\circ$ values were observed for the BPDE- and FBPDE-modified duplexes.

Discussion

It was our aim to prepare fluoro-BPDEs that are conformationally and metabolically compatible to unmodified BPDEs. Replacement of hydrogens within the benzo ring of BP (i.e., C_{6,8,9,10}) with fluorine atoms can alter its metabolic pathways, DNA binding behavior, and tumorigenicity (18, 35, 52). Similar observations have been made for benz[*a*]anthracene derivatives (53, 54). For example, it has been shown that fluorine substitution at position 6 of BP perturbs the BP 7,8-diol conformation (15, 16, 52). Thus, it is necessary to insert fluorine at sites distal to the diol epoxide region of BP (i.e., C1, -2, or -3). Our motivation for the fluorine substitution at C2 was primarily a synthetic one, i.e., ease of constructing the 2-fluorobenzo[*a*]pyrenyl system via a Friedel-Crafts reaction of 2-fluoropyrene. Importantly, the diol epoxide conformation is not likely to be altered by fluorine substitution at a remote C2 position. Although 1-fluoropyrene was readily available as a starting material, its use resulted in a mixture of regioisomers that did not meet our needs (Figure 2).

Synthesis. We described the synthesis of *RSSR*- and *SRRS*-*anti*-FBPDE (**22** and **23**, respectively). As detailed in Figures 3 and 4, the synthesis entailed 15 steps starting from the commercially available pyrene. The highlights of the synthesis are the regiospecific succinylation of 2-fluoropyrene, followed by stereospecific 7,8-dihydrodiol functionalization (30–32). Subsequent mCPBA epoxidation of the resulting dihydrodiol produced the chiral *anti*-diol epoxides (34–38). The stereochemistry of the catalyst-controlled reaction sequence was in accordance with the metabolic activation of BP (1, 5, 6). Thus, the *R,R*-Jacobsen catalyst generated the sequence of (*7S,8S*)-*trans*-dihydrodiol/(*7S,8R,9R,10S*)-*anti*-FBPDE, whereas the *S,S*-catalyst resulted in the opposite stereochemistry, (*7R,8R*)-*trans*-dihydrodiol/(*7R,8S,9S,10R*)-*anti*-FBPDE (Figure 4) (30, 31). Our NMR (³J_{7,8}) analysis, CD spectra, and charge density data all indicate that both *anti*-FBPDE and *anti*-BPDE preferentially adopt the pseudo-diequatorial diol conformation. The presence of fluorine at the C2 position was monitored by measuring ¹⁹F NMR spectra throughout the synthesis.

CD. The CD spectra were extremely valuable for determining the absolute configuration and conformation of all of the FBP intermediates as well as the monomeric (FBP-*N*²-dG) and oligomeric adducts (8, 43–51). As discussed above, the Jacobsen catalyst-controlled stereochemical sequence mimics the *in vivo* metabolism of BP. In general, the CD profiles of the FBP- and BP-diol derivatives were very similar, indicating that the fluorine substitution at C2 did not alter the conformation of FBPDE. A close interaction between the pyrene chromophore

and the chiral substituents at C7,8 is responsible for the three major groups of CD signals in the 250–400 nm range (Figure 5). Signals centered around ~340 and ~290 nm arise from the longitudinal and transverse transition dipole moments of the pyrene ring, while signals below 275 nm could involve both transitions (8, 34). While some differences in magnitude and range emerged, the elliptic orientations for each enantiomeric pair were always opposite each other (Figure 5). Thus, the 7*S*,8*S*-stereoisomers always exhibit a $-/+/-$ pattern, whereas the 7*R*,8*R*-counterparts show a $+/-/+$ pattern in the 250–400 nm region. An exception was the reversal of the observed CD patterns between the tetrahydro (**12/14**) and the dihydro (**19/21**) derivatives. A similar pattern switch has been observed previously for the nonfluoro BP-7*R*,8*R*-diol sequence (34). The nature of the substitution at C7,8 greatly influenced the magnitude of the longitudinal ellipticities (e.g., 300–375 nm). Also, the intense signals above 300 nm for the dihydrodiols **19/21** reflect the contribution of the extended C9,10 π -electrons to the longitudinal pyrenyl transition.

The CD spectrum is an excellent tool for investigating PAH-diol conformation. The CD profile of the FBP-7*R*,8*R*-dihydrodiol (**21**) is almost a mirror image of the corresponding 6- and 9-fluoro-BP and is nearly identical to that of the BP-7*R*,8*R*-dihydrodiol (33–35). These results indicate that the isosteric fluorine substitution at C2 does not alter the 7,8-diol conformation (i.e., pseudo-equatorial). The stereochemical characterization of the tetraols was also aided by CD analysis. Each of the enantiomeric *anti*-FBPDE was hydrolyzed to produce a mixture of the early eluting major and the late eluting minor peaks, which were designated as *trans*-tetraols and *cis*-tetraols (*trans*-*anti* and *cis*-*anti*), respectively (Figure 9). The CD spectra of the early eluting major products, *RSRS*- and *SRSR*-*ta*-FBPT, were mirror images of each other (Figure 5e). A similar result was obtained from the late eluting tetraols, *RSRR*- and *SRSS*-*ca*-FBPTs (Figure 5f). The results establish unambiguously the enantiomeric relationships of these products.

DNA Adducts. Each of the *anti*-FBPDE was reacted with dGMP or two 11-mer oligodeoxynucleotides to produce the corresponding monomer *N*²-dG and the oligonucleotide adducts (5'-CCATXG*CTACC-3' where G* = FBP-*N*²-dG adduct; X = dT, oligo I; X = dC, oligo II). We designated the early eluting major fractions from the dGMP reaction as *trans*-opened FBP-*N*²-dG adducts on the basis CD and ESI-MS analyses. Three **22**-*trans*-FBP-oligo II, **23**-*trans*-FBP-oligo II, and **22**-*trans*-FBP-oligo I of the four possible oligo adducts were isolated in sufficient quantities to enable characterization (ESI-TOF-MS, enzyme digest/HPLC, and CD spectra). The purified oligonucleotides were annealed with the appropriate complementary sequences (**22**-*trans*-FBP-duplex II, **23**-*trans*-FBP-duplex II, and **22**-*trans*-FBP-duplex I) for UV melting and CD experiments. The results were in accordance with those obtained previously from the corresponding BPDE duplexes in the same sequence contexts (51). We also observed that, unlike the controls, increasing the temperature (45–85 °C) resulted in the formation of several isosbestic points in the CD spectra of FBP-modified duplexes. It is interesting to note that the effect was greater for those modified with **22** regardless of sequence. The results indicate that the dynamics of helix–coil transition of the FBP-modified duplexes are sensitive to the nature of adduct structure (i.e., stereochemistry). Pradhan et al. (50, 51) have observed a temperature dependence (5–45 °C) of the near-UV absorption and ICD characteristics of all of the stereoisomers of BPDE-*N*²-dG complexes in various sequence contexts. It has been shown that the DNA duplexes containing *anti*-*trans*-BP-*N*²-dG

adopt predominantly minor groove conformations, although a possible coexistence of intercalative binding was implicated in the $-TG^*C-$ sequence context (9).

In summary, we report here the preparation and characterization of (+)- and (–)-*anti*-FBPDEs and their dG and oligonucleotide adducts. Comparative CD spectra analysis and UV melting analyses indicated that the *anti*-FBPDEs prepared in our laboratory are conformationally and thermodynamically comparable to the unmodified *anti*-BPDEs at the diol epoxide and DNA adduct levels (FBP-*N*²-dG, FBP-duplex DNA). These results support the utility of FBPDEs as useful structural probes. Currently, we are scaling preparation of the FBP-modified DNA for future NMR work.

Acknowledgment. We are grateful to the NIH (R01CA-098296) for their financial support for this work. This research was made possible in part by the use of the Research Core Facility supported by the NCR/NIH (P20 RR016457). We thank M. P. Chiarelli for measuring the ESI-MS-TOF spectra of FBP-modified oligonucleotides. We thank K. Overly for providing the comparative DFT B3LYP/6-31G* calculations of *SRRS*-*anti*-FBPDE and *SRRS*-*anti*-BPDE. We also thank B. Zajc for critical reading of the manuscript.

Supporting Information Available: Details of synthesis, parameters of duplex formation, HPLC and online UV spectra, HPLC chromatograms, and ¹H NMR, ¹³C NMR, and ESI-MS spectra. This material is available free of charge via the Internet at <http://pubs.acs.org>.

References

- Xue, W., and Warshawsky, D. (2005) Metabolic activation of polycyclic and heterocyclic aromatic hydrocarbons and DNA damage: A review. *Toxicol. Appl. Pharmacol.* 206, 73–93.
- Kriek, E., Rojas, M., Alexandrov, K., and Bartsch, H. (1998) Polycyclic aromatic hydrocarbon-DNA adducts in humans: Relevance as biomarkers for exposure and cancer risk. *Mutat. Res.* 400, 215–231.
- Boysen, G., and Hecht, S. S. (2003) Analysis of DNA and protein adducts of benzo[a]pyrene in human tissues using structure-specific methods. *Mutat. Res.* 543, 17–30.
- Poirier, M. C., and Weston, A. (1996) Human DNA adduct measurements: State of the art. *Environ. Health Perspect.* 104, 883–893.
- Harvey, R. G. (1991) *Polycyclic Aromatic Hydrocarbons: Chemistry and Carcinogenicity*, Cambridge University Press, Cambridge, England.
- Dipple, A. (1994) In *DNA Adducts: Identification and Biological Significance* (Hemminki, K., Dipple, A., Segerback, D., Kadlubar, F. F., Shuker, D., and Bartsch, H., Eds.) pp 107–129, IARC Scientific Publications, Lyon, France.
- Beland, F. A., and Kadlubar, F. F. (1990) In *Handbook of Experimental Pharmacology* (Cooper, C. S., and Grover, P. L., Eds.) Vol. 94/I, pp 267–325, Springer-Verlag, Heidelberg.
- Szeliga, J., and Dipple, A. (1997) DNA adduct formation by polycyclic aromatic hydrocarbon dihydrodiol epoxides. *Chem. Res. Toxicol.* 11, 1–11.
- Geacintov, N. E., Cosman, M., Hingerty, B. E., Amin, S., Broyde, S., and Patel, D. J. (1997) NMR solution structures of stereoisomeric covalent polycyclic aromatic carcinogen-DNA adducts: Principles, patterns, and diversity. *Chem. Res. Toxicol.* 2, 111–146.
- Patel, D. J., Mao, B., Gu, Z., Hingerty, B. E., Gorin, A., Basu, A. K., and Broyde, S. (1998) Nuclear magnetic resonance solution structures of covalent aromatic amine-DNA adducts and their mutagenic relevance. *Chem. Res. Toxicol.* 11, 391–407.
- Cho, B. P. (2004) Dynamic conformational heterogeneities of carcinogen-DNA adducts and their mutagenic relevance. *J. Environ. Sci. Health, Part C* C22, 57–90.
- Yan, S., Wu, M., Buterin, T., Naegeli, H., Geacintov, N. E., and Broyde, S. (2003) Role of base sequence context in conformational equilibria and nucleotide excision repair of benzo[a]pyrene diol epoxide-adenine adducts. *Biochemistry* 42, 2339–2354.
- Zhou, L., Rajabzadeh, M., Trafficante, D. D., and Cho, B. P. (1997) Conformational heterogeneity of arylamine-modified DNA: ¹⁹F NMR evidence. *J. Am. Chem. Soc.* 119, 5384–5389.

- (14) Cho, B. P., and Zhou, L. (1999) Probing the conformational heterogeneity of the acetylaminofluorene-modified 2'-deoxyguanosine and DNA by ^{19}F NMR spectroscopy. *Biochemistry* 38, 7572–7583.
- (15) Zajc, B. (1999) Synthesis of (\pm)-*trans*-7,8-dihydrodiol of 6-fluorobenzo[*a*]pyrene via hydroxyl-directed regioselective functionalization of substituted pyrene. *J. Org. Chem.* 64, 1902–1907.
- (16) Yagi, H., Sayer, J. M., Thakker, D. R., Levin, W., and Jerina, D. M. (1987) Effects of a 6-fluoro substituent on the solvolytic properties of the diastereomeric 7,8-diol 9,10-epoxides of the carcinogen benzo[*a*]pyrene. *J. Am. Chem. Soc.* 109, 838–846.
- (17) Mulder, P. P. J., RamaKrishna, N. V. S., Cremonesi, P., Rogan, E. G., and Cavalieri, E. L. (1993) Synthesis of 1- and 3-fluorobenzo[*a*]pyrene. *Chem. Res. Toxicol.* 6, 657–661.
- (18) Fu, P. P., Von Tungeln, L. S., Chiu, L.-H., and Own, Z. Y. (1999) Halogenated-polycyclic aromatic hydrocarbons: A class of genotoxic environmental pollutants. *Environ. Carcinog. Ecotoxicol. Rev. C17*, 71–109.
- (19) Bergmann, E. D., Selig, H., and Lin, C.-H. (1975) Reaction of xenon difluoride with polycyclic aromatic hydrocarbons. Fluorination of pyrene. *J. Org. Chem.* 40, 3793–3794.
- (20) Streiweiser, A., Jr., Lawler, R. G., and Schwaab, D. (1965) On the bromopyrenes. *J. Org. Chem.* 30, 1470–1493.
- (21) Bavin, P. M. G. (1959) 4-Nitropyrene. *Can. J. Chem.* 37, 1614–1615.
- (22) Bolton, R. (1964) Tetrahydropyrene as a source of 2-pyrenyl derivatives. *J. Chem. Soc.* 4637–4638.
- (23) Connor, D. M., Allen, S. D., Collard, D. M., Liotta, C. L., and Schiraldi, D. A. (1999) Efficient synthesis of 4,5,9,10-tetrahydropyrene: A useful synthetic intermediate for the synthesis of 2,7-disubstituted pyrenes. *J. Org. Chem.* 64, 6888–6890.
- (24) Musa, A., Sridharan, B., Lee, H., and Mattern, L. (1996) 7-amino-2-pyrenecarboxylic acid. *J. Org. Chem.* 61, 5481–5484.
- (25) Miller, D. W., Herreno-Saenz, D., Huang, K. H., Heinz, T. M., and Fu, P. P. (1992) Synthesis of nitropolycyclic aromatic hydrocarbons with the substituent at the longest axis. *J. Org. Chem.* 57, 3746–3748.
- (26) Zhou, L., and Cho, B. P. (1998) Comparative conformational analyses of *N*-(deoxyguanosin-8-*yl*)aminopyrene adducts derived from the isomeric carcinogens 1-, 2-, and 4-Nitropyrene. *Chem. Res. Toxicol.* 11, 35–43.
- (27) Ansell, L. L., Rangarajan, T., Burgess, W. M., Eisenbraun, E. J., Keen, G. W., and Hamming, M. C. (1976) The synthesis of 1,2,3,7,8,9-hexahydrodibenzo[*def, mno*]chrysene and the use of hydriodic acid-*ri* phosphorus in the deoxygenation of ketones. *Org. Prep. Proc. Int.* 8, 133–140.
- (28) Fu, P. P., and Harvey, R. G. (1977) Synthesis of the diols and diol epoxides of carcinogenic hydrocarbons. *Tetrahedron Lett.* 18, 2059–2062.
- (29) Harvey, R. (1985) Synthesis of the dihydrodiol and diol epoxide metabolites of carcinogenic polycyclic hydrocarbons. *ACS Symp. Ser.* 283, 35–62.
- (30) Harvey, R. G., and Tang, X. (1995) Enantioselective synthesis of the tumorigenic anti-diol epoxide metabolites of benzo[*a*]pyrene. *Tetrahedron Lett.* 36, 2737–2740.
- (31) Huang, X., and Harris, T. M. (1995) Enantioselective synthesis of the (+)-anti-7,8-dihydrodiol-9,10-epoxide of the potent carcinogen benzo[*a*]pyrene. *J. Chem. Commun.* 1699–1700.
- (32) Jacobsen, E. N., and Zhang, W. (1990) Enantioselective epoxidation of unfunctionalized olefins catalyzed by salen manganese complexes. *J. Am. Chem. Soc.* 112, 2801.
- (33) Harvey, R. G., and Cho, H. (1977) Efficient resolution of the dihydrodiol derivatives of benzo[*a*]pyrene by high-pressure liquid chromatography of the related (–)-dimenthoxyacetates. *Anal. Biochem.* 80, 540–546.
- (34) Nakanishi, K., Kalsai, H., Cho, H., Harvey, R. G., Jeffrey, A. M., Jennette, K. W., and Weinstein, I. B. (1977) Absolute configuration of a ribonucleic acid adduct formed in vivo by metabolism of benzo[*a*]pyrene. *J. Am. Chem. Soc.* 99, 257–258.
- (35) Chiu, P. L., Weems, H. B., Wong, T. K., Fu, P. P., and Yang, S. K. (1983) Stereoselective metabolism of benzo[*a*]pyrene and 7-methylbenzo[*a*]pyrene by liver microsomes from sprague-Dawley rats pretreated with polychlorinated biphenyls. *Chem.-Biol. Interact.* 44, 155–168.
- (36) Harvey, R. G. (1989) Conformational analysis of hydroaromatic metabolites of carcinogenic hydrocarbons and the relation of conformation to biological activity. In *Conformational Analysis of Cyclohexenes, Cyclohexadienes, and Related Hydroaromatic Compounds* (Rabideau, P. W., Eds.) pp 267–298, VCH Publishers, New York.
- (37) Yagi, H., Hernandez, O., and Jerina, D. M. (1975) Synthesis of (\pm)-7 β ,8 α -dihydroxy-9 β ,10 β -epoxy-7,8,9,10-tetrahydrobenzo[*a*]pyrene as potential metabolites of the carcinogen benzo[*a*]pyrene with stereochemistry related to the antileukemic tripolides. *J. Am. Chem. Soc.* 97, 6881–6883.
- (38) Yagi, H., Thakker, D. R., Hernandez, O., Koreeda, M., and Jerina, D. M. (1977) Synthesis and reactions of the highly mutagenic 7,8-diol 9,10-epoxides of the carcinogen benzo[*a*]pyrene. *J. Am. Chem. Soc.* 99, 1604–1611.
- (39) McCaustland, D. J., and Ebgel, J. F. (1975) Metabolites of polycyclic aromatic hydrocarbons. II. Synthesis of 7,8-dihydrobenzo[*a*]pyrene-7,8-diol and 7,8-dihydrobenzo[*a*]pyrene-7,8-epoxides. *Tetrahedron Lett.* 16, 2549–2552.
- (40) Beland, F. A., and Harvey, R. G. (1976) The Isomeric 9,10-oxides of *trans*-7,8-dihydroxy-7,8-dihydrobenzo[*a*]pyrene. *J. Chem. Soc. Chem. Commun.* 84–85.
- (41) Lehr, R. E., Schaefer-Ridder, M., and Jerina, D. M. (1977) Synthesis and reactivity of diol epoxides derived from non-K-region trans-dihydrodiols of benzo[*a*]anthracene. *Tetrahedron Lett.* 18, 539–542.
- (42) Kong, J., White, C. A., Krylov, A. I., Sherrill, C. D., Adamson, R. D., Furlani, T. R., Lee, M. S., Lee, A. M., Gwaltney, S. R., Adams, T. R., Ochsenfeld, C., Gilbert, A. T. B., Kedziora, G. S., Rassolov, V. A., Maurice, D. R., Nair, N., Shao, Y., Besley, N. A., Maslen, P. E., Dombroski, J. P., Daschel, H., Zhang, W., Korambath, P. P., Baker, J., Byrd, E. F. C., Van Voorhis, T., Oumi, M., Hirata, Hsu, S., C.-P., Ishikawa, N., Florian, J., Warshel, A., Johnson, B. G., Gill, P. M. W., Head-Gordon, M., and Pople, J. A. (2000) Q-Chem 2.0: A high-performance ab initio electronic structure program package. *J. Comput. Chem.* 21, 1532–1548.
- (43) Peltonen, K., Cheng, S. C., Hilton, B. D., Lee, H., Cortez, C., Harvey, R. G., and Dipple, A. (1991) Effect of bay region methyl group on reactions of *anti*-benzo[*a*]anthracene 3,4-dihydrodiol 1,2-epoxides with DNA. *J. Org. Chem.* 56, 4181–4188.
- (44) Vepachedu, S. R., Ya, N., Yagi, H., Sayer, J. M., and Jerina, D. M. (2000) Marked differences in base selectivity between DNA and the free nucleotides upon adduct formation from Bay- and Fjord-region diol epoxides. *Chem. Res. Toxicol.* 13, 883–890.
- (45) Chang, H.-F., Huffer, D. M., Chiarelli, M. P., and Cho, B. P. (2002) Characterization of DNA adducts and tetraols derived from anti-benzo[*ghi*]fluoranthene-3,4-dihydrodiol-5,5a-epoxide. *Chem. Res. Toxicol.* 15, 187–197.
- (46) Chang, H.-F., Huffer, D. M., Chiarelli, M. P., Blankenship, L. R., Culp, S. J., and Cho, B. P. (2002) Characterization of DNA adducts derived from syn-benzo[*ghi*]fluoranthene-3,4-dihydrodiol-5,5a epoxide and comparative DNA binding studies with structurally related anti-diolepoxides of benzo[*ghi*]fluoranthene and benzo[*c*]phenanthrene. *Chem. Res. Toxicol.* 15, 198–208.
- (47) Ponten, I., Seidel, A., Graslund, A., and Jernstrom, B. (1996) Synthesis and characterization of adducts derived from the syn-diastereomer of benzo[*a*]pyrene 7,8-dihydrodiol 9,10-epoxide and the 5'-d(CCTATA-GATATCC) oligonucleotide. *Chem. Res. Toxicol.* 9, 188–196.
- (48) Cosman, M., Ibanez, V., Geacintov, N. E., and Harvey, R. G. (1990) Preparation and isolation of adducts in high yield derived from the binding of two benzo[*a*]pyrene-7,8-dihydroxy-9,10-oxide stereoisomers to the oligonucleotide d(ATATGTATA). *Carcinogenesis* 11, 1667–1672.
- (49) Pradhan, P., Jernstrom, B., Seidel, A., Norden, B., and Graslund, A. (1998) Induced circular dichroism of benzo[*a*]pyrene-7,8-dihydrodiol 9,10-epoxide stereoisomers covalently bound to deoxyribonucleotides used to probe equilibrium distribution between groove binding and intercalative adduct conformations. *Biochemistry* 37, 4664–4673.
- (50) Pradhan, P., Jernstrom, B., Seidel, A., Norden, B., and Graslund, A. (1999) Studies on the adduct heterogeneity of benzo[*a*]pyrene 7,8-dihydrodiol 9,10-epoxide stereoisomers covalently bound to deoxyribonucleotides by induced circular dichroism and light absorption spectroscopy. *Chem. Res. Toxicol.* 12, 403–411.
- (51) Arghavani, M. B., SantaLucia, J., Jr., and Romano, L. J. (1998) Effect of mismatched complementary strands and 5'-change in sequence context on the thermodynamics and structure of benzo[*a*]pyrene-modified oligonucleotides. *Biochemistry* 37, 8575–8583.
- (52) Chou, M. W., and Fu, P. P. (1984) Stereoselective metabolism of 8- and 9-fluorobenzo[*a*]pyrene by rat liver microsomes: Absolute configurations of *trans*-dihydrodiol metabolites. *J. Toxicol. Environ. Health* 14, 211–223.
- (53) Harvey, R. G., and Cortez, C. (1997) Fluorine-substituted derivatives of the carcinogenic dihydrodiol and diol epoxide metabolites of 7-methyl-, 12-methyl-, and 7,12-dimethylbenzo[*a*]anthracene. *Tetrahedron* 53, 7101–7118.
- (54) Baer-Dubowska, W., Nair, R. V., Dubowski, A., Harvey, R. G., Cortez, C., and DiGiovanni, J. (1996) The effect of fluoro substituents on reactivity of 7-methylbenzo[*a*]anthracene diol epoxides. *Chem. Res. Toxicol.* 9, 722–728.